AD-A050 175 CALIFORNIA INST OF TECH PASADENA DEPT OF ELECTRICAL --ETC F/G 20/12
ANALYSIS OF SEMICONDUCTOR STRUCTURES BY NUCLEAR AND ELECTRICAL --ETC(U)
JUL 77 K N TU, J W MAYER F19628-75-C-0008
UNCLASSIFIED SCIENTIFIC-5 RADC-TR-77-254 NL

END
DATE FILMED
3-78
DDC

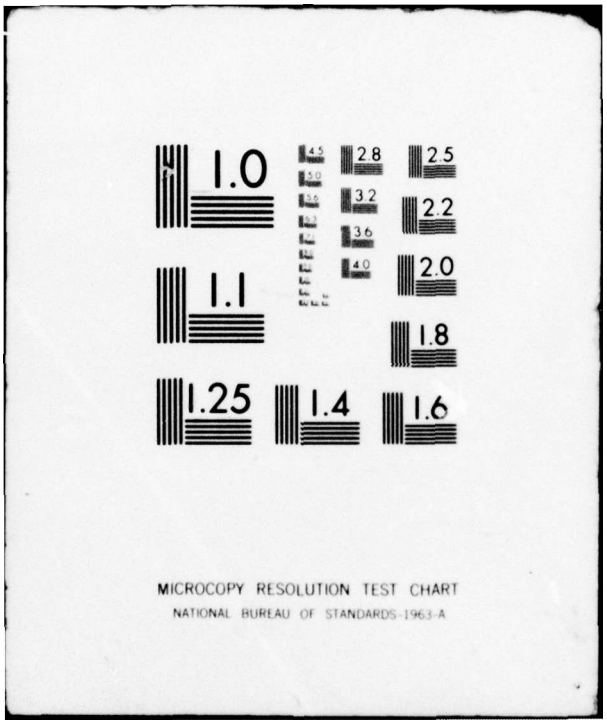
1.0
1.1
1.25
1.4
1.6
1.8
2.0
2.2
2.5
2.8
3.2
3.6
4.0
4.5
5.0
MICROCOPY RESOLUTION TEST CHART
NATIONAL BUREAU OF STANDARDS-1963-A

RADC-TR-77-254
Interim Scientific Report
July 1977

ANALYSIS OF SEMICONDUCTOR STRUCTURES BY NUCLEAR AND ELECTRICAL TECHNIQUES

California Institute of Technology

ROME AIR DEVELOPMENT CENTER
AIR FORCE SYSTEMS COMMAND
GRIFFISS AIR FORCE BASE, NEW YORK 13441

This report has been reviewed by the RADC Information Office (OI) and is releasable to the National Technical Information Service (NTIS). At NTIS it will be releasable to the general public, including foreign nations.

This technical report has been reviewed and approved for publication.

APPROVED: D. Eirug Davies

D. EIRUG DAVIES
Project Engineer

APPROVED: Robert M. Barrett

ROBERT M. BARRETT
Director
Solid State Sciences Division

FOR THE COMMANDER: John P. Huss

Plans Office

SECURITY CLASSIFICATION OF THIS PAGE (When Data Entered)

REPORT DOCUMENTATION PAGE	READ INSTRUCTIONS BEFORE COMPLETING FORM
1. REPORT NUMBER: RADC-TR-77-254	2. GOVT ACCESSION NO. / 3. RECIPIENT'S CATALOG NUMBER
4. TITLE (and Subtitle): ANALYSIS OF SEMICONDUCTOR STRUCTURES BY NUCLEAR AND ELECTRICAL TECHNIQUES	5. TYPE OF REPORT & PERIOD COVERED: Scientific Report No. 5
	6. PERFORMING ORG. REPORT NUMBER
7. AUTHOR(s): King N. Tu, James W. Mayer*	8. CONTRACT OR GRANT NUMBER(s): F19628-75-C-0008
9. PERFORMING ORGANIZATION NAME AND ADDRESS: California Institute of Technology, Electrical Engineering Department, Pasadena, California 91125	10. PROGRAM ELEMENT, PROJECT, TASK AREA & WORK UNIT NUMBERS: 61102F, 2305J101, J1
11. CONTROLLING OFFICE NAME AND ADDRESS: Deputy for Electronic Technology (RADC/ESO), Hanscom AFB, MA. 01731, Monitor: D. Eirug Davies	12. REPORT DATE: July 1977
	13. NUMBER OF PAGES: 75
14. MONITORING AGENCY NAME & ADDRESS (if different from Controlling Office): Technical Rept.	15. SECURITY CLASS. (of this report): Unclassified
	15a. DECLASSIFICATION/DOWNGRADING SCHEDULE

16. DISTRIBUTION STATEMENT (of this Report)

Distribution unlimited; approved for public release. 77 p.

17. DISTRIBUTION STATEMENT (of the abstract entered in Block 20, if different from Report)

18. SUPPLEMENTARY NOTES

*IBM, Thomas J. Watson Research Center, Yorktown Heights, NY 10598
** California Institute of Tech, Division of Engineering and Applied Science Pasadena, California 91125

19. KEY WORDS (Continue on reverse side if necessary and identify by block number)

Silicide Formation
Thin Metal Film Reactions with Si Substrate
Analysis of Product
Marker Motion
Mechanism of Silicide Formation

20. ABSTRACT (Continue on reverse side if necessary and identify by block number)

This report is an overview of the subject of silicide formation by thin metal films reacting with a Si substrate.

The first section discusses the method of sample preparation typically used in the studies of silicide formation. The experimental techniques applied to analyze the resulting compound layers are described, and their advantages and limitations are discussed. Three specific cases are reviewed in detail (Ni, Hf, V). They fall in a general pattern of silicide formation (metal-rich silicides, monosilicides, disilicides). Oxidizing ambients during the anneal-

next page

DD FORM 1 JAN 73 1473 EDITION OF 1 NOV 65 IS OBSOLETE

UNCLASSIFIED

SECURITY CLASSIFICATION OF THIS PAGE (When Data Entered)

404 888

ing can interfere with the kinetics, but do not appear to affect the final composition of the compounds formed.

The second section treats marker experiments of various kinds (implanted inert gas atoms, deposited inert metal islands, radioactively marked atoms and compound layers). The results of these experiments are discussed, and it is shown how atomic diffusivities can be derived from marker experiments.

The third section deals with the formation process itself. The role of the solubilities and diffusivities of the elements in each other, and in the compounds, are discussed. The energy of formation of the silicides are compared with the types of silicides actually observed. It is noted that kinetics of atomic movements and the crystal structure of the compounds must be considered to come to an understanding of the silicides observed. A central question is that of nucleation and which phase the nucleation process will favor.

The work points out the need for a better understanding of the marker experiments of the microstructure of the silicides and their dominant defects, as well as a clarification of the process of nucleation

TABLE OF CONTENTS

1 Introduction

The recent impetus for studying silicide formation is due to the requirements placed on the performance of integrated circuits. It now appears that one of the limiting factors in achieving high production yield and high device reliability lies in the choice of the metallization scheme. The problem arises from the requirements for a controlled contact at the semiconductor-metal interface and for a low resistance metal that does not lead to voltage drop across the contact. One must realize that there are practical reasons for the choice of a particular metallization scheme. A concept which is feasible under research laboratory conditions may not be adaptable to production requirements where high yield is required. The metallization must also be compatable with the processing temperature and packaging structure. Since every production line has a somewhat different process control it is difficult to give specific details on all the constraints imposed on the metallization. Instead we will give some general guidelines for the selection of metals used to make contacts.

Figure 1 shows schematically an FET with a heavily doped source and drain and a lightly doped channel connecting the source and drain. The contact to the source and drain and to the channel may have a different structure but ideally the same metallization is used for both. In early devices, the junction regions made by diffusion were located several microns below the surface. There were not many constraints on metallization other than adhesion, barrier height, low electrical resistance and high corrosion resistance. In these aspects, aluminum was ideal. Because of

the relatively large device dimensions, the dissolution of Si into Al and the consequent penetration into Si around the periphery of the contact caused relatively few problems in shorting the junction. However, as device dimensions decrease and junction depths become shallow it is obvious that the Al penetration problem can no longer be tolerated.

The design philosophy next introduced was to use a silicide forming metal (1-4) to produce a uniform layer with controlled barrier height and good adhesion to Si and then a second metal, typically Al, Au or W to provide the low resistance path. The thickness of the silicide layer is typically less than 1000Å and only a few hundred Å of Si is consumed in forming the silicide. The purpose of the silicide layer is not only to provide a good Schottky barrier but also to prevent the reaction between Al and Si. But unfortunately, Al also reacts with silicide layer (5,6) and hence a diffusion barrier layer must be interposed between the silicide and the Al. This structure is shown in the insert in Fig. 1. In order to give a feeling of how such a three-layer structure is fabricated, we show some typical processing steps in Fig. 2. Again we emphasize that each production line may use a slightly different temperature and sequence, and the lithography, etching and pattern definition steps also differ from one production line to another. We will show only the general principles in the following.

The metallization process step used in forming the gate contact to the channel region of an FET is shown in Fig. 2. Before deposition, Fig. 2a, there is a native oxide layer on the Si surface in the window opened by etching the thick oxide layer. It is this native oxide layer which has caused many of the problems associated with contact metallization. One of the requirements for any contact metal is that the metal must be

able to penetrate this oxide layer whose thickness may range between 15 to 50Å. It has been found that some metals, such as Pt and Pd, can readily penetrate this thin oxide layer to form silicide layers.

We will illustrate the metallization scheme by platinum silicide which is probably the most generally used contact material in integrated circuits. During the deposition of Pt, the substrate is sometimes maintained at an elevated temperature around 300°C and subsequently sintered at an elevated temperature of 550°C to complete the silicide formation. After sintering, the structure shown in Fig. 2b is composed of a thin silicide layer (about 1000Å thickness for a 500Å Pt layer) with a thin oxide on top. This thin oxide layer is composed of elements either from the original native oxide layer, or introduced during deposition and sintering. (7) Since silicon is a necessary ingredient in the formation of this oxide layer and since Pt does not react with thick SiO_2 layers, the layer is formed only above the silicide region but not on the Pt layer over the thick oxide. The excess Pt is removed by aqua regia etching. The thin oxide layer prevents dissolution of the silicide during the aqua regia etching step.

In the next general step, the thin oxide layer is removed with a buffered HF solution, then the barrier and Al layer are deposited. In general, another heat treatment step around 450°C is required at this point to penetrate any oxide layer between the metal films and to produce a low resistance contact. It is because of this second heat treatment step that the barrier layer is introduced to prevent the Al from penetrating the Pt silicide layer.

The general requirement for any contact is that there must be a

uniform and limited reaction between the two layers in contact. A reaction is required to make sure that there is an intimate contact and adhesion. We use the word "limited" to imply that there is no long range atomic migration that could lead to film penetration or junction shorts. The requirement for uniformity arises from the fact that deep penetration can start at localized points due to interface instability. If such localized penetration does occur, severe pitting will result since all the reaction produced must originate from a localized region. This is referred to as a spike formation. Figure 3 shows two SEM pictures of spike formation around the periphery of a contact area. (7a) These pictures were obtained from a specimen of Al on Si which was sintered at 450°C for 1 hour in N_2 ambient and followed by the removal of the metal electrode.

In the following sections we will neglect many of the problems encountered in the lithography used in pattern formation in order to emphasize the major features of silicide formation; mechanism of phase formation, kinetics of reaction in terms of time and temperature, reaction with oxide layer and influence of oxygen in the ambient.

Although we have emphasized the technological aspects of silicide formation, the reactions between transition metals and silicon are of interest in their own right. In contrast to the case of bimetallic thin film reactions, in silicide formation, one deals with a fine-grained metallic thin film in contact with a single crystal covalently bonded semiconductor. One might anticipate that the crystal orientation and the microstructure of silicide might play a role. Since it is known

that silicide formation can occur at a temperature as low as 100°C, (8-9), it is also interesting to investigate the physical mechanism which is responsible for breaking the covalent bonds in Si. At this low reaction temperature, the growth phase may be determined by the reaction kinetics rather than thermodynamic driving forces.

2 Analysis of Silicide Formation

2.1 Sample Preparation

In this section we adopt a different viewpoint than that for device production and consider the most basic aspects of silicide formation. Rather than follow the constraints imposed by production requirements with narrow openings in the oxide layer and the associated stress and coverage problems around the periphery of the openings, we deal with large area deposition. Then too we assume that enough effort has been made to remove interfacial oxide and to achieve oxygen free thin film deposition. In subsequent heat treatments, either a vacuum better than 10^{-6} Torr or a purified flowing atmosphere of He or other inert gas is used. Although all these precautions may not reproduce the exact situation in the production line, they do make it possible to achieve reproducible experimental results. We will return to the discussion of practical aspects of silicide formation in the end of this section.

Typically the thin films are deposited in a electron beam deposition system under dry conditions. Although elevated temperature substrates are sometimes employed, often the substrates are maintained at ambient temperature during deposition. The film thickness generally ranges from 500 to 2000Å. The substrates are in most cases Si wafers with a polished surface of device quality such as those used in integrated circuit device

fabrication. Immediately before being placed in the deposition chamber, the wafers are immersed in a buffered HF solution and rinsed by deionized H_2O and blown dry. In certain situations, the wafers are sputter etched before metal deposition when it is suspected that the native oxygen on the wafer may interfere with the silicide formation. (10)

2.2 *Experimental Analysis Techniques*

The analytical techniques used to determine the structure of deposited films and phase changes resulting from heat treatment have been described by a number of authors in the open literature. Obviously, it is advantageous to apply more than one analytical technique to analyze any given film structure. Rather than describing all the different techniques again, we will only mention some of the more common techniques used today in the majority of silicide studies. We will not describe these techniques in detail but will try to cover some of the strong points and limitations of these techniques from the standpoint of information that can be gained from silicide formation.

Identification of phases is provided by glancing angle x-ray diffraction. The diffraction patterns can be obtained either in a camera or a diffractometer. (11,12) The advantages of a camera are simplicity and speed. As shown in Fig. 4 which is an x-ray diffraction pattern of a NiSi film obtained with a Read camera, (12) it has sufficient sensitivity to identify phases present in films a few thousand Å thick. Quantitative information about peak intensity and line broadening as well as phase identification can be provided by a diffractometer. Figure 5 shows a glancing angle x-ray diffraction spectrum from Ni deposited on Si and heat treated at 250°C for 24 hours. The Ni_2Si phase can be identified by

more than 12 of its reflections. Also present in the spectrum are reflections of the residue Ni, but no reflections of other phases can be detected.

The sensitivity of both glancing angle x-ray techniques is approximately 200Å. Consequently in utilization of x-ray diffraction we are studying the growth phase of the silicide which has a thickness dimension over 200Å. This growth phase is not necessarily the first phase nucleated at the metal-silicon interface during the initial heat treatment. To study the very early stage of growth, transmission electron microscopy (TEM) could be used. At present, such a study has not been carried out and the TEM technique has been used primarily in microstructure measurement and identification of defects and epitaxial orientation relations. (13-15) Figure 6 shows transmission electron micrographs and diffraction patterns of thin Ni_2Si films grown on (100) and (111) Si.

To obtain growth kinetics and the chemical composition of the phases, it is customary to use Rutherford ion backscattering (16) or Auger electron spectroscopy (AES) combined with sputtering. (17) The advantage of Rutherford backscattering is that it provides a fast measurement of the thickness and composition of the growth phase. From spectra such as shown in Fig. 7, one can measure the energy width of the phase to determine its thickness and the ratio of the spectrum heights in the Ni and Si signals to give the composition ratio.

A limitation of backscattering is that it is difficult to make a positive identification of composition of phases of less than 200Å thick when they are located at the metal-Si interface

several thousands Å below the top surface of the metallic film. In this respect again, we investigate the growth phase of silicide formation rather than the nucleation of the silicide.

The backscattering technique is not sensitive to the presence of low mass impurities in the silicide. This information as well as the thickness and composition of silicide can be obtained from AES measurements. The Auger depth profiles of a sample of Ni on Si before and after the reaction at 250°C for 1 hour to form Ni_2Si are shown in Fig. 8. In these profiles, there are problems associated with establishing the absolute depth scale and ensuring that the sputtering does not change the composition of the eroded surface. On the other hand, it is possible to look at the shifts in the peak position in the Auger spectrum to obtain information on the chemical bonds of the species. To date the fullest advantage of this approach has not been taken.

2.3 Examples of Silicide Formation

Three examples of silicide formation are given in the following. The formation of nickel silicides will be discussed first and followed by hafnium silicide and vanadium silicide. The growth of silicides in these three examples are quite different. The first phase formation in the nickel case is a nickel-rich silicide, Ni_2Si. In the case of hafnium, it is the monosilicide, HfSi, forms first. However, vanadium is found to react with Si to form disilicide, VSi_2, without being preceded by the formation of a monosilicide or a metal-rich silicide.

2.3a Nickel on Silicon

The formation of nickel silicide between a film of Ni and a Si wafer exhibits a sequential growth of three phases; Ni_2Si, NiSi and $NiSi_2$. (18)

Figure 9 shows examples in which Ni_2Si and NiSi are formed. At higher temperatures $NiSi_2$ is formed and has been shown to grow epitaxially on Si. The growth of the phase Ni_2Si is initiated at the interface between Ni and Si at temperatures from 200°C to 350°C as shown in Fig. 9. The growth kinetics of Ni_2Si follows a parabolic relation between thickness of Ni_2Si and annealing time as shown in Fig. 10. One also observes that the growth rate of Ni_2Si at 275°C is a factor of 2 greater on (100) oriented Si substrates than on (111) substrates. TEM studies have indicated that there is a difference in the microstructure of silicide formed on (100) and (111) Si. (15) The activation energy of the formation of Ni_2Si has a value of 15 ± 0.2 eV over the temperature range from 200°C to 325°C, see Fig. 11. This figure shows that the activation energies do not differ remarkably between (100) and (111) Si.

Similar studies of kinetics have not been carried out for the growth of the two higher temperature phases, NiSi and $NiSi_2$. The transformation of Ni_2Si into NiSi is initiated at the interface between Si and Ni_2Si. The transformation is found to accompany a stress change from compression in Ni_2Si to tension in NiSi. (19) The stress level is about 10^{10} dynes/cm^2. The formation of NiSi is very fast at temperatures above 350°C and the phase is stable up to 750°C. At higher temperature than 750°C epitaxial growth of $NiSi_2$ has been found on (111), (110) and (100) Si. The epitaxial orientation relationship has been determined by channeling studies using MeV He ion and by reflection electron diffraction. (18)

2.3b Hafnium on Silicon

The reaction of Hf with Si represents a case where the metal-rich silicides shown in the equilibrium phase diagrams are not the growth phase

observed. (10) The reaction occurs at a much higher temperature than that for the growth of metal-rich silicides, such as Ni_2Si, and the first phase formed is the monosilicide, HfSi. The monosilicide is stable from 525°C to 700°C and at temperatures from 750°C to 990°C it transforms to the disilicide, $HfSi_2$.

The growth kinetics for the formation of HfSi are shown in Fig. 12 for a 1500Å Hf film on (100) and (111) Si. The growth follows a parabolic relation and there is no pronounced influence of the substrate orientation on the formation kinetics. The activation energy for HfSi growth was determined to be 2.5 eV as shown in Fig. 13. This activation energy is about 1 eV larger than that found for the case of Ni_2Si.

The formation of $HfSi_2$ is different from that of HfSi which forms as a uniform layer between the hafnium and silicon. The disilicide $HfSi_2$ does not form a uniform layer but rather grows in randomly localized regions throughout the HfSi. (10) Because of this non-uniform growth, it was not possible to determine the growth kinetics.

2.3c Vanadium on Silicon

The reactions of V with Si produces the disilicide as the only growth phase. (20,21) The initial growth of VSi_2 follows a linear growth rate as shown in Fig. 14. For longer times there is a deviation from the linear growth rate. It was found that the presence of oxygen can slow down the growth rate of VSi_2, so it was suggested that the deviation shown in Fig. 14 was due to contamination of oxygen introduced into the film during deposition and subsequent anneals. A general consequence of a linear growth behavior is that the linear region will gradually change to

a parabolic region when the growth becomes limited by diffusion through the growth layer. However in the case of the growth of VSi_2, experiments with films containing different impurities showed that the departure from linear growth was due to the presence of impurities.

The formation of vanadium silicide represents the situation where the end phase, the disilicide, is also the dominant growth phase. In the other examples cited in the above, the formation of disilicide was preceded by the formation of a monosilicide or a metal-rich silicide. Of the examples shown, the growth of VSi_2 was the only case in which a linear rather than a parabolic growth rate was found.

2.4 Summary of Silicide Formation

In the phase diagrams of metal-Si systems, in general, there are more than three silicides formed. One general observation is that not all the equilibrium phases are present as the dominant growth phase during silicide formation in thin film systems. We do not imply that some of the equilibrium phases can not nucleate but only that they do not grow to a macroscopic dimension greater than the few hundred Å which can be detected by the techniques mentioned in the previous section. The examples shown in the preceding sections were chosen as representative of the three broad classes of silicide formation observed in structures composed of metal thin films on single crystal silicon; the metal-rich silicide, typically M_2Si, the monosilicide, MSi and the disilicide, MSi_2.

Table I shows the general pattern of silicide formation. The silicides listed in the right hand columns are chosen as specific examples of the phase formation for the elements shown in the left column. The phase formation proceeds from left to right in each row with the more

metal-rich silicide forming first. In all cases, the final phase (most right-handed entry in each row in the Table) represents the end phase between Si and the metal shown in the equilibrium phase diagram. For the case of Mg only one phase is found in the phase diagram. For the refractory metals, many phases exist in their phase diagram (22), yet only the disilicide is found.

2.4a Metal-rich Silicides

A survey of silicide formation in metal-rich silicides is given in Table II. One notes that the growth kinetics follows a parabolic law with an activation energy around 1.5eV. The formation temperature for all five silicides starts around 200°C with the notable exception of Co_2Si which is at 350°C. At the present time, we do not know the reason for this high formation temperature and note that silicide formation of Co_2Si has been checked independently in three different laboratories (Caltech, IBM, Phillips). On the other hand all the surface preparation and deposition systems were basically the same and it is possible that an alternative preparation technique might lead to a lower formation temperature.

2.4b Monosilicides

The formation of monosilicides shown in Table III is also characterized by a parabolic growth rate with an activation energy of 1.6 to 2.5eV. The latter number appears higher than the general trend. The formation temperature for monosilicides is higher than that for the metal-rich silicide and generally occurs above 350°C. A notable exception is PdSi which forms above 700°C. This must imply that the precursary phase Pd_2Si is extremely stable. We comment that in at least three

cases, Ni, Co and Pt, it is possible to have the metal-rich silicide formed as a layer between the metal and the monosilicide. In other cases, such as Hf and Rh, the monosilicide is the first phase growth observed in the silicide. In the case of Ti, it is the disilicide that is generally observed as the growth phase. However, x-ray diffraction has recently indicated that TiSi is formed prior to the growth of the disilicide. (23)

2.4c Disilicides

Table IV summarizes the formation of the disilicide phase observed in the growth of silicide layers. The formation temperature is around 600°C except for $CrSi_2$ which forms around 450°C. The activation energy of formation is high, ranging from 1.7 to 3.2eV. The disilicides of three metals, Ni, Co and Fe are found to grow epitaxially on Si substrates. In these cases, the disilicide has a close lattice match with the Si.

The disilicide of the refractory metals tends to have a linear growth curve in the early stage of reaction when it is the first growth phase. It is difficult in some cases to obtain a clean measurement of the growth kinetics because of the influence of oxygen contamination as found for VSi_2 and $CrSi_2$. For refractory metals, the presence of a thin interfacial oxide layer between the metal and Si can impede the silicide formation as has been directly shown in the case of Cr on Si.

2.5 Practical Aspects

In this section, we would like to return to a few practical aspects of silicide formation that are encountered either in the production environment or in the choice of a metallization scheme. We will not cover

all aspects since each device has its own particular requirements, further, we will not cover some areas such as corrosion, adhesion, lithographic and lift-off steps. Instead we will treat two topics in which there have been some published work related to the basics of silicide formation as discussed in the preceding sections.

2.5a Oxygen Ambient

Oxygen and water vapor are universal contaminants in deposition systems and thermal processing ambients. We have earlier pointed out that the presence of oxygen in a metal film can retard the growth of the silicide. A more general phenomenon is the presence of some oxygen in the heat treatment processing atmosphere. Since silicon oxidizes readily, one may anticipate that oxide layers are formed at the top surface of silicide layer when oxygen or water vapor are present.

It has been clearly established that oxide layers are formed near the top surface of PtSi. (24) As we have pointed out in section 1 the presence of this oxide layer is often used to protect the PtSi during etching processes.

If excessive amounts of oxygen are present in the heat treatment ambient it is possible to form an oxide layer well below the Pt surface. (7) The structure of the silicide layer is shown in Fig. 15 for silicide layers either formed in an oxygen ambient or post-annealed in oxygen. The presence of such oxide layers below the Pt surface can lead to undesirable side effects such as poor adhesion and poor electrical contact. This outer Pt and oxide layer must be etched away before the next metal layer deposition. The formation of oxide layers is a rather

general phenomena during silicide formation and one must anticipate that oxide layer removal steps should be included in the development of silicide as one of the metallization steps.

2.5b Reaction with Oxide Layer

Many of the transition elements can form silicides when in contact with SiO_2 as well as Si. We can broadly classify the reaction between metals and SiO_2 as shown in Table V, Gold shows no tendency to form oxide and Au-silicides are unstable. However, gold in contact with thin oxide layers can cause dissolution of the oxide when heated above the Au-Si eutectic point. The mechanism is that Au penetrates the thin oxide and reacts with the underlying Si layer to form a eutectic in liquid form which wets the SiO_2 and leads to dissolution. (25,26) Aluminum on the other hand can form an oxide layer and when Al is deposited on SiO_2 a strong adhesion is obtained. We suspect that this is due to the reaction between Al and SiO_2 to form the strong Al-O bonds at the interface.

Pt and Pd themselves do not form oxide layers easily and consequently their adhesion to thick layers of SiO_2 is rather poor. However, when these metals are in contact with a thin native oxide on Si, silicide formation can still occur at low temperatures. In these cases, we believe the reaction is similar to that with Au in that the Pt or Pd can penetrate the thin oxide layer and form a silicide at the Si-oxide interface and at the same time break up the oxide. But if the oxide is too thick it will form a diffusion barrier to prevent the silicide from formation.

The refractory metals such as Cr, Ti and V form both oxides and silicides. When deposited on thick oxide layers they develop strong adhesive

bonds. In fact Cr and Ti are often used as a glue layer between oxide layer and less adhesive metals. On the other hand, since these metals do form oxide layers the metal oxide becomes a diffusion barrier for further reaction between the metal and SiO_2. It has been shown that silicide layers can be formed under this condition but generally at temperatures 100°C to 200°C above that where the metal reacts with bare Si, i.e. 700 to 900°C rather than 600°C. In addition (20,21,27) the silicide formed is generally metal-rich, for example, V_3Si is formed rather than VSi_2. Table VI summarizes the reaction products of Ti, V and Nb on Si and SiO_2 substrates. Marker experiments (see next section) on the reaction between V and SiO_2 has shown that V is moving species in V_3Si formation (28) rather than Si as was found in VSi_2. We believe that this represents a rather general condition where the metal species must diffuse through the growing metal-rich silicide so that the metal atoms can reach the reaction front at the silicide-SiO_2 interface.

3 Marker Motion

3.1 Ideal Marker

In our discussion so far we have not identified whether Si or metal atoms move across the silicide layer during the growth of the layer. The fact that growth occurs implies that one or both of the species are transported to either the metal-silicide or Si-silicide interface. However, it is impossible to determine the identity of the diffusing species without some form of marker experiments.

The initial experiments with a diffusion marker were carried out in bulk samples by Kirkendall and Smigelskas. (49) In these bulk diffusion couples, the faster of the diffusing species is identified by the direc-

tion of displacement of embedded wire markers of mils in diameter. In thin films which are a few thousand Å thick, the concept of embedded wire marker must be scaled down in dimension. One requires markers that are a few hundred Å in dimension that do not influence the kinetics of silicide growth. Ideally, the marker should also be inert, i.e. should not react with Si or the metal at the silicide growth temperature, and should remain immobile as the diffusing species streams by.

An additional constraint is that the marker should be located within the silicide layer to avoid possible influence due to the presence of interfaces. As shown in Fig. 16, if the metal atoms are the diffusing species, the marker will be displaced toward the top surface of the film. Conversely, if Si atoms are predominantly the moving species, the marker will be displaced deeper into the sample. If both species are moving, it is possible to have relatively small displacement of the marker during the silicide growth. Under this condition, as shown by Darken's analysis (50), the relative displacement of the marker can be used to determine the difference in the fluxes of the two diffusing species.

3.2 Interface Drag

If the marker is located near the interface, the marker can be dragged along by the interface irrespective of the direction of the net flux of the diffusing species. Figure 17 shows an idealized case with a spherical marker located at the interface between the Si and the silicide layer. Since the interface moves as a result of reaction occuring at the interface, the question whether or not the marker can be buried within the silicide depends upon the relative magnitude of interfacial energies "σ" per unit area in the vicinity of the marker. If the following energy equation is

satisfied, the marker will be dragged by the advancing interface.

$$2\pi r^2\sigma_1 + \pi r^2\sigma_2 \leq 2\pi r^2\sigma_3 \qquad (1)$$

where r is the radius of the spherical marker and σ_1, σ_2 and σ_3 are the specific interfacial energies between Si and marker, Si and silicide, and silicide and marker, respectively. In other words, even if the metal atoms are the diffusing species, the marker can be dragged deeper into the sample if too much energy is required to break away from the interface. An associated phenomenon is found in oxidation of silicon where n-type dopants are dragged by the advancing oxide front deeper into the sample. (51) This snow-plow effect is caused by the small solubility of the dopant within the oxide layer. However, at the relatively low temperatures of silicide formation, it is not appropriate to consider the solubility of the marker where as in high temperature oxidation the segregation effect can play a significant role.

Let us consider a marker located at the Si-silicide interface which moves with the interface. We will show that it is impossible to determine which species is moving across the silicide layer during growth. If Si is the dominant diffusing species, growth of the silicide occurs at the metal-silicide interface and some motion of Si occurs at the boundary of the marker as shown in Fig. 18a. This is the situation predicted even if no marker-drag occurs. If the metal atoms are the diffusing species and interface drag occurs, silicide growth takes place at the silicon-silicide interface and also at the marker-silicide interface. To accomplish this again some Si transport must occur around the boundary of the marker, as shown iin Fig. 18b. The net results, however, is that the marker is displaced deeper into the sample as would have occurred if Si atoms were the

diffusing species.

Similar argument can be applied to the metal-silicide interface. If marker drag occurs, it is still not possible to determine which species is moving across the silicide. These arguments imply that if the marker position coincides with the interface position during silicide growth, one must be cautious about interpreting the identity of the diffusing species.

3.3 Actual Experiments

In practice, there are experimental difficulties associated with introducing a detectable marker into a thin film structure. One of the difficulties is to achieve the right dimension of the marker and another is to avoid forming an oxide layer at the position of the marker. In the latter case, it is not easy to do processing of a silicide, to introduce a marker and then to redeposit a metal for subsequent reaction. This approach is generally tried first; however, it has been observed that the reaction stops at the interface between the oxide and the newly deposited metal. We can anticipate that sputter cleaning before metal deposition could be used to overcome the problem associated with the oxide. To date, there have been two concepts that have been applied to inert marker study: implantation of inert gas atoms (52) and deposition of a discontinuous W layer. (53)

3.3a Implanted Marker

In this work an inert gas such as Ar or Xe is implanted into the Si surface. The Si sample must then be annealed to temperatures above 600°C to reorder the implanted layer and remove the major amount of implantation induced defect structures. During this heat treatment, it has been shown for the case of Xe that Xe bubbles of 50Å to 100Å in

diameter are formed. (54) After this implantation step the Si surface must be etched to remove any oxide or hydrocarbon layers. Following the surface cleaning step, a metal layer is deposited on the sample. Figure 19 shows in the uppper portion the backscattering spectra from a Xe marker implanted sample of Ni on Si before and after the formation of Ni_2Si. After silicide formation, the Xe marker is buried within the silicide and displaced toward the surface. The lower portion of Fig. 19 shows the amount of the displacement of the Xe marker against the silicide thicknesses. These results show that interface drag did not occur and Ni is the dominant diffusing species.

If Si is the moving species, when the advancing silicide front reaches the implanted marker, the marker will move deeper into the sample at the position of the interface. To determine the identity of the moving species it is then necessary to implant markers into the deposited metal layer. Then during silicide growth, as the silicide-metal interface advances to the marker, if the marker becomes buried, its position will be shifted deeper into the sample, indicating that Si is the dominant diffusing species.

With high energy implantation, 0.5 to 10 MeV, it is possible to partially form the silicide and then implant through the remaining metal into the silicide. To date there have been no reported results of this method of marker implantation within the silicide layer.

One of the disadvantages in using backscattering techniques to detect the implanted marker is that the atomic mass of the marker atoms must be selected so that the signal from the marker occurs in a region in the energy spectrum that is free from the signal from the Si or the metal

atoms. Preliminary experiments have shown that this problem can be overcome by the use of Auger depth profiling measurements.

3.3b Deposited Marker

Another approach is to deposit small and isolated islands of an inert metal on the Si surface followed by a cleaning of the Si surface and deposition of the silicide forming metal. The islands of the metal marker must have sufficient adherence to the Si so that they remain intact during the surface cleaning step. These islands must also be small in size and should not react with either the Si or the silicide forming metal at the growth temperature.

Van Gurp et al (53) deposited a thin Sn film which forms islands upon deposition, then a 30Å W film was deposited and the Sn island dissolved. This leaves patches of W in the regions between the original Sn islands. After this, Co was deposited on the sample surface and the formation of Co_2Si was carried out at temperatures from 400°C to 500°C. The growth kinetics in this sample was the same for those samples without a W layer except that the growth starts after an incubation period of 1 to 10 minutes. During formation of the silicide layer, the position of W marker shifted toward the surface at the position of the Co_2Si-metal interface. This experiment shows that it is possible to deposit a metal film which does not interfere with the silicide formation. However, further experiments are required to show that interface drag effect do not control the marker motion.

3.3c Radioactive Marker

A tracer technique using radioactive ^{31}Si has been applied to study the nature of mass transport during the solid phase epitaxial growth of

Si on <100> Si with amorphous Si as a source layer and Pd_2Si compound as an intermediate layer. (55) The tracer was obtained by neutron activation in a nuclear reactor and has a half-life time of 2.62 hours by emitting beta radiation. By determining the position change of the tracer before and after the epitaxial growth, it is found that the supply of Si to the growth comes indirectly from the dissociation of the Pd_2Si rather than directly from the amorphous Si.

Whether the tracer Si can be used as a diffusion marker in silicide formation is an interesting question, and some preliminary results of using tracer Si as a diffusion marker in the formation of Pd_2Si, Ni_2Si and Co_2Si have been obtained. (56) These results showed that the tracer Si has taken part in the reaction of silicide formation, so it is not an inert marker and can not be used to determine whether the metallic or the Si is the dominant diffusion species. Nevertheless, it is found that at low temperatures if the interdiffusion of Si takes place by grain boundary diffusion, the tracer Si within silicide grains becomes inert, then it should be possible to differentiate mass transport in the lattice from along grain boundaries by determining the position change of the tracer atoms. It seems that more work using this kind of marker is desirable.

3.3d Intermediate Silicide Layer

There have been several cases where an intermediate silicide layer is formed such as NiSi between Ni_2Si and Si or Pd_2Si between Si and

$CrSi_2$. (57) It is tempting to describe the formation of the outer silicide layer, for example $CrSi_2$ on top of Pd_2Si, as being due to the transport of Si through the intermediate silicide, Pd_2Si in this case. This conclusion can not be supported because it is possible that the intermediate silicide can dissociate giving up Si atoms to form $CrSi_2$ and releasing Pd atoms to diffuse through the remaining Pd_2Si to form a new layer of Pd_2Si at the Si-Pd_2Si interface.

3.4 Diffusing Species

Table VII lists the silicides in which the diffusing species have been identified by means of marker experiments. From the Table, one notices that metal atoms diffuse in the cases where the metal-rich silicide M_2Si is formed. In fact for the three silicides, Ni_2Si, Mg_2Si and Co_2Si the metal is the dominant diffusing species. Conversely, in the case where the disilicide is formed, silicon is the diffusing species. We believe that the same pattern will be found in other disilicides if marker experiments are carried out.

For the case of monosilicides, Si is again the dominant diffusing species. For the three cases listed, the monosilicide was the first phase formed. Marker experiments have not yet been performed in those monosilicides which form after the metal-rich silicide.

There is a consequence to the silicide growth when one species dominates in the diffusion. Vacancy accumulation should occur at the Si-silicide interface if Si is the diffusing species. This might lead to poor silicide adhesion and impaired electrical contact. Such effect has been found with W on SiGe alloy. (60)

3.5 Marker Analysis

In the last section, the application of marker studies has been used mainly to identify the dominant diffusion species during silicide formation. It is well known from Darken's analysis (50) of marker motion in bulk diffusion couples (49,61,62) that the intrinsic diffusion coefficient of each species can be determined from marker measurements, so there is more information than identification of the dominant diffusion species that can be extracted from a marker study. For details of Darken's analysis, readers are referred to the original paper (50), Chapter 5 in Shewmon's (63) or in Manning's (64). In extending Darken's analysis to marker study in silicide formation, we realize that there are two outstanding features of silicide formation that require attention. First, we are dealing with a diffusion couple that forms compounds rather than solid solution. At the interfaces where discontinuity of structure and composition occurs the lattice is being destroyed and created at the same time, so the continuity equation or Fick's second law can not be applied there. Instead, we must use a growth equation. Second, the interdiffusion coefficient, $\tilde{D}$, in Darken's analysis is measured typically by the use of Boltzmann-Matano solution, so the equation

$$\tilde{D} = D_1 \frac{C_2}{C} + D_2 \frac{C_1}{C} \tag{2}$$

can be combined with the marker motion equation,

$$v = \frac{1}{C} (D_1 - D_2) \frac{dC_1}{dx} \tag{3}$$

to unravel D_1 and D_2 from $\tilde{D}$. Here, D_1 and D_2 are the intrinsic diffusion coefficient of component 1 and 2 in the alloy of composition

$C=C_1+C_2$, respectively. v is the drift velocity measured by a marker in a coordination with the origin located at one end of the couple where no interdiffusion takes place. However, in a diffusion controlled growth of silicide, we do not measure $\tilde{D}$ by the use of Boltzman-Matano solution but rather we measure typically a kinetic parameter "A" from the rate of growth of the layer based on the relation that

$$x^2 = At \tag{4}$$

where x and t are layer thickness and time of growth, respectively. In general, A is similar to a diffusion coefficient, nevertheless it does not equal $\tilde{D}$. Thus we must find out how A is related to the intrinsic diffusion coefficients D_1 and D_2. We should point out that Kidson (65) has shown an analysis of layer growth and obtained an analytical solution of A as a function of $\tilde{D}$. Although it is a rather complicated solution, it relates A to D_1 and D_2 indirectly through $\tilde{D}$. In the following, we shall take Kidson's approach of layer growth and extend it to include marker motion.

In Fig. 20, a schematic phase diagram and concentration profile of the metallic element during the formation of a silicide layer between the metal and Si is shown. In the figure and equations that follow, α, β and δ represent the Si, silicide, and metal phase, respectively. Also the superscript "1" stands for metal and "2" for silicon. At the interface between α and β, the growth equation takes the following form

$$(C^1_{\beta\alpha} - C^1_{\alpha\beta})\left(-\frac{d\xi_{\alpha\beta}}{dt}\right) = J^1_{\beta\alpha} - J^1_{\alpha\beta} \tag{5}$$

where

$$J^1_{\beta\alpha} = -D^1_\beta \left.\frac{dC^1_{\beta\alpha}}{dx}\right|_{\alpha\beta} + v_{\alpha\beta}C^1_{\beta\alpha} \tag{6}$$

and

$$J^1_{\alpha\beta} = - D^1_\alpha \left.\frac{dC^1_{\alpha\beta}}{dx}\right|_{\alpha\beta} + v_{\alpha\beta} C^1_{\alpha\beta} \tag{7}$$

are the flux terms. $\frac{d\xi_{\alpha\beta}}{dt}$ is the growth velocity of the $\alpha\beta$ interface. $v_{\alpha\beta}$ is drift velocity of the silicide layer as a whole measured at the $\alpha\beta$ interface. D^1_α and D^1_β are intrinsic diffusion coefficients of the metal in α and β, respectively. Substituting Eqs. (6) and Eq. (7) into Eq. (5), we have

$$-\frac{d\xi_{\alpha\beta}}{dt} = \frac{-D^1_\beta \left.\frac{dC^1_{\beta\alpha}}{dx}\right|_{\alpha\beta} + D^1_\alpha \left.\frac{dC^1_{\alpha\beta}}{dx}\right|_{\alpha\beta}}{C^1_{\beta\alpha} - C^1_{\alpha\beta}} + v_{\alpha\beta} \tag{8}$$

Similarly, at the $\beta\gamma$ interface, we have

$$\frac{d\xi_{\beta\gamma}}{dt} = \frac{-D^1_\gamma \left.\frac{dC^1_{\gamma\beta}}{dx}\right|_{\beta\gamma} + D^1_\beta \left.\frac{dC^1_{\beta\gamma}}{dx}\right|_{\beta\gamma}}{C^1_{\gamma\beta} - C^1_{\beta\gamma}} + v_{\beta\gamma} \tag{9}$$

Since the concentration variation across the silicide layer is not large, the drift velocities $v_{\alpha\beta}$ and $v_{\beta\gamma}$ are practically equal. Then if we follow Kidson's analysis and take

$$K^1_{ij} = \frac{dC^1_{ij}}{d\lambda}$$

to be constant at the ij interface, where $\lambda = \frac{x}{\sqrt{t}}$, we obtain, by combining Eq. (8) and Eq. (9) and upon integration, the following equation

$$(\xi_{\beta\gamma} - \xi_{\alpha\beta}) = 2\sqrt{t}\left\{\frac{-(D_\gamma K)^1_{\gamma\beta} + (D_\beta K)^1_{\beta\gamma}}{C^1_{\gamma\beta} - C^1_{\beta\gamma}} + \frac{-(D_\beta K)^1_{\beta\alpha} + (D_\alpha K)^1_{\alpha\beta}}{C^1_{\beta\alpha} - C^1_{\alpha\beta}}\right\} + x_m \tag{10}$$

where $\xi_{\beta\gamma} - \xi_{\alpha\beta} = W_\beta$ is the layer thickness of the β phase, and x_m is the marker displacement, ($2vt = x_m$).

Equation (10) can be simplified in certain special cases. In the case where one species is found to be the dominant diffusion species, such as Ni during the growth of Ni_2Si, the growth takes place mainly at one of the interfaces, the $\alpha\beta$ interface. Then we can assume $J^1_{\gamma\beta} \approx J^1_{\beta\gamma}$ and neglect the first term on the right hand side of Eq. (10). Furthermore, if a plot of $\ell n\ (W_\beta - x_m)$ against $\frac{1}{T}$ shows that the relation is linear, it means either the activation energies are about the same or one of the terms is dominant. Now, if we assume that $D^1_\beta K^1_{\beta\alpha}$ is dominant over $D^1_\alpha K^1_{\alpha\beta}$, we obtain a simplified form of Eq. (10) in the following

$$W_\beta - x_m = 2t^{1/2} \frac{-D^1_\beta K^1_{\beta\alpha}}{C^1_{\beta\alpha} - C^1_{\alpha\beta}} \tag{11}$$

When the same assumptions are applied to Kidson's equation of layer growth, (65) we again obtain a simplified form for the layer growth where one species dominates the diffusion,

$$W_\beta = 2t^{1/2} \frac{-\tilde{D}_\beta K^1_{\beta\alpha}}{C^1_{\beta\alpha} - C^1_{\alpha\beta}} \tag{12}$$

where $\tilde{D}_\beta$ has the following form (see Eq. (2)).

$$\tilde{D}_\beta = D^1_\beta \frac{C^2_\beta}{C_\beta} + D^2_\beta \frac{C^1_\beta}{C_\beta}$$

and

$$C_\beta = C^1_\beta + C^2_\beta \ .$$

By subtracting Eq. (11) from Eq. (12), we have

$$v = \frac{C^1_\beta}{C^1_{\beta\alpha} - C^1_{\alpha\beta}} \frac{1}{C_\beta} \ (D^1_\beta - D^2_\beta) \ \frac{d\, C^1_{\beta\alpha}}{dx}\Bigg|_{\alpha\beta} \tag{13}$$

We note that $C^1_\beta \simeq C^1_{\beta\alpha} - C^1_{\alpha\beta}$, so Eq. (13) in fact has the same form as Eq. (3). What is being shown here is that Eq. (11) and (12) can be reduced back to Eq. (2) and (3).

Combining Eq. (11) and Eq. (12), we can determine D^1_β and D^2_β provided that the other parameters can be measured. Among them, the measurement of $K^1_{\beta\alpha}$ may require some clarification. Since it represents the driving force of the diffusion, it is directly related to the formation energy, ΔH, of silicide in the case of silicide formation. The formation energy of silicide will be discussed in the next section.

Using the simple relation that $\mu = RT \ln C$ where μ is chemical potential in the usual sense, we obtain

$$K_{ij} = \frac{\sqrt{t}}{RT} C_{ij} \left(\frac{\Delta\mu}{\Delta x}\right)_{ij} \tag{14}$$

For a first order approximation, we can take $\Delta\mu$ to be ΔH, the formation energy of silicide as given in Table IX. Then, in the case of growth of Ni_2Si (ΔH = 11.2 Kcal/mole) as reported in Fig. 2a in Ref. 52, we found the diffusivity of Ni and Si in Ni_2Si at 325°C to be

$$\begin{aligned} D_{Ni} &= 1.7 \times 10^{-14} \text{ cm}^2/\text{sec} \\ D_{Si} &= 0.6 \times 10^{-14} \text{ cm}^2/\text{sec} \end{aligned} \tag{15}$$

which show that in Ni_2Si the Ni atoms diffuse faster than the Si by a factor of 3. If marker motion data at other temperatures become available, we can then determine the diffusion activation energy and pre-exponential factor for the Ni and Si separately. On the other hand, using the activation energy of 1.5 eV given in Table II for interdiffusion in Ni_2Si, we obtain a diffusivity at 325°C of the same order as

those given in Eq. (15) provided that the pre-exponential factor is about 0.1 to 0.01. These values seem reasonable in view of the crude treatment given above.

4 Mechanism of Silicide Formation

4.1 Introduction

From the viewpoint of phase transformation, silicide formation as presented in this chapter concerns the reaction between two solid phases in direct contact to form ordered intermetallic compounds at temperatures well below the formation of any liquid phase. The reaction is unique in that it occurs between two different kinds of solids: the substrate is covalently bonded single crystal and the thin film is metallic and fine-grained. From the summary given in section 2.4, one finds the formation of three classes of silicides; metal-rich silicides, monosilicides and disilicides. Typically, with some scattering of data, they start to form around 200°C, 400°C and 600°C, respectively. The mechanism of silicide formation must take into account the large temperature differences.

Since the metallic films are fine-grained, we expect that a fast mass transport of metallic atoms can occur at their grain boundaries. Even for those high melting point refractory metals, this also seems plausible because the reaction temperature of 600°C is high enough for grain boundary diffusion to take place. The observation that all the first phase disilicides of refractory metals start to form around 600°C is striking in view of the large variation of melting point of the metals. This suggests that the supply of refractory metal atoms is not rate limiting. Otherwise a much wider range of formation temperature should have been found. On the other hand, the formation of metal-

rich silicides at 200°C which is about 0.3 of the absolute melting point of Si raises the question that how can Si atoms break away from its lattice at such a low temperature. It seems then the supply of Si is crucial to silicide formation. The mechanism of Si supply at high temperatures might very well be different from that at low temperatures. At temperatures as low as 200°C, phonon energy is not sufficient to dissociate the covalent bonds in Si, so other mechanisms to free a Si from its lattice must be invoked.

While the kinetic data shows the large variation in silicide formation and allows us to classify the silicides accordingly, the mechanisms of formation can not be understood without also knowing the thermodynamic data of silicides since the driving force behind the formation comes from free energy change. In Fig. 21, the equilibrium binary phase diagram of Ni-Si is shown. The diagram shows that there are six Ni-Si intermetallic compounds that can exist below the lowest eutectic point in the system. The compound which is next to Si is $NiSi_2$ and is the stable phase (the end phase) to be expected when the reaction is complete. Since Ni is shown to have a solubility of Si up to several percent, the formation of the end phase could be preceded by solution or by the formation of the other phases. However, substitutional solution can only occur when lattice diffusion (via vacancies) takes place. Hence at low reaction temperatures, the formation of the other phases is more likely. Here a difficult question arises as to whether we can predict the first phase nucleation and growth. In the following, we shall first discuss the thermodynamic data, then the kinetic mechanism of silicide formation, and finally the problems of predicting first phase nucleation.

4.2 Thermodynamic Data of Metal-Si Systems

4.2a The End Phase

The end phase of silicides which is stable with Si for various metallic elements was first given systematically using the periodic table by Lepselter and Andrews. (1) Figure 22 is a reproduction of theirs with a minor change. The Au is now shown to form a metastable metal-rich silicide with Si. (66) A trend that can be seen in Fig. 22 is that from left to right the end phases shows an increase in its metal concentration; disilicide, monosilicide, metal-rich silicide, and finally metal with a small amount of Si as solute. An obvious correlation to the trend is the lowering of melting point of these end phases, but other than that, whether it has any correlation to the mechanism of silicide formation is not at all clear at present.

4.2b Solubility and Diffusivity

The solubility of Si in metallic elements can be simply presented by using the Darken-Gurry plot, (67) which is reproduced in Fig. 23. The metallic elements are classified into four groups according to their solubility of Si as given in the insert on the upper right corner. Elements such as Ni, Co, Fe and V that possess a large solubility of Si are scattered close to Si in the plot, and those that are immiscible with Si are found to locate far away from Si. Data of solubility is important in determining whether there is dissolution before silicide formation. In reacting Ni and V with Si, no noticeable solution of Si in these metals was found preceding the silicide formation. But Si was found to disolve into Fe film up to 25 at. % at 400°C before the formation of FeSi takes place. (40)

The plot can not be used to deal with the solubility of metallic elements in Si. One reason is that the plot was constructed by using the atomic radius of Si of 12 coordinations. It is known, with no exceptions, that Si has an extremely small solubility of metallic elements. Yet, such a low solubility limit is hard to reach at low temperatures if the solute has to take substitutional sites in Si by a vacancy mechanism of diffusion. This is due to the high formation energy of vacancy in Si. On the other hand, there are metals which are known to be fast diffusants in Si with an activation energy of about leV. (68) Table VIII lists the available data of self and some solute diffusion in Si. Most of these data were obtained by tracer technique using Si samples at equilibrium state with no excess point defects. The Table shows that the noble and near noble metals can diffuse in Si much faster than Si itself. The fast diffusion can occur at a temperature as low as 200°C, and it is most likely by a dissociative interstitial diffusion. No diffusion data of refractory metals in Si is available. One measurement of Ti diffusion in Ge showed that it is slower than Ge self ddiffusion. (69) Because of their high valence electrons and large atomic size, refractory metals are expected to dissolve and diffuse substitutionally in Si (Cr might be an exception). Since a substitutional diffusion will require an activation energy comparable to that of self diffusion, refractory metals therefore are not expected to dissolve into Si at temperatures such as 200°C.

4.2c Formation Energy of Silicide

Table IX lists the free energy of formation of silicides expressed in units of kcal/g-atom. (80-82) The middle column in the Table shows the

silicides of Ti and Zr, and they are characterized by a larger formation energy of monosilicide than that of disilicide. The right hand column are silicides of the rest of the refractory metals and is characterized by having no monosilicide (except CrSi) and also by the large formation energy of the disilicide. For example, VSi_2 is found to have the largest formation energy per g-atom among all the silicides in Table IX. Compared to other disilicides, the formation energy seems surprisingly high. From the summary given in section 2.4, the temperature of disilicide formation for these metals is about 600°C. At this temperature, if we assume that the kinetics is fast, i.e. not a limiting factor and so energy change will dictate the selection of silicide formation, the disilicide is favored. Indeed, disilicide is the only observed growth phase for these metals. For silicides of Ti, Zr and Hf, the formation of TiSi and HfSi occurs at temperatures above 500°C. The formation of these monosilicides is not only favored by their high energy of formation but also by their simpler crystal structure as compared to that of disilicides. The unit cell of monosilicide of Ti, Zr and Hf (FeB type) has 8 atoms while the unit cell of their disilicide (C49 type) has 12 atoms. Although the energy of formation of these two unit cells are about the same, the monosilicide is kinetically favored because of lesser number of atoms involved in the nucleation and growth. In a few cases, the silicide M_5Si_3, where M stand for the refractory metals, is shown in Table IX to have a higher formation energy than that of monosilicide or disilicide. But the formation of this silicide can only occur when the supply of Si is limited, otherwise, it is obvious that the formation of five molecules of monosilicide or disilicide is energetically more favorable than the formation of one molecule of M_5Si_3.

The left hand column in Table IX gives the formation energy of silicides of other transition metals and Mg. Here, no obvious trends can be given based on the energies. However, the metal-rich silicides are characterized by their low temperature formation. At a low temperature, whether atoms can jump or not often plays a more significant role in controlling the formation than the available energy change. The mechanism of formation of these metal-rich silicides will be discussed later.

4.2d Interfacial Energy

During a single phase silicide formation, the three interfaces of our concern are the metal-silicon, metal-silicide, and silicide-silicon interfaces. The nucleation of a silicide can be better understood if we know the magnitude of these interfacial energies, yet unfortunately, there is no such data in the literature. Also the growth rate of a silicide may depend on the structure of its interfaces. Since the Si substrate is a single crystal, the silicide that grows epitaxially on the Si could develop a coherent or semicoherent interface with the Si, depending on the amount of mismatch. For example, Pd_2Si is known to grow epitaxially on the (111) surface of Si with a very small mismatch, so their interface can be regarded as coherent. A coherent interface is low in free energy; this may be one of the reasons for the rather easy formation of Pd_2Si during the deposition and its rather high stability with respect to the transformation to PdSi. On the other hand, the epitaxial growth raises a question concerning how the interface can maintain its coherency while moving into the (111) Si. A further discussion of this question will be given later.

4.3 Kinetic Mechanism of Silicide Formation

The crucial step in the kinetics of silicide formation is how to main-

tain the supply of Si by breaking the bonds in the substrate. For the formation of disilicide of refractory metals, the bond-breaking probably takes place at weak spots on silicon surface such as kinks and ledges. Thus a high reaction temperature is required to supply to a phonon the needed energy to free those surface atoms. Hence, the thickening rate of disilicide at the early stage of growth is linear, and marker studies show that Si atoms are the dominating diffusing species. For the formation of metal-rich silicide of near noble metals, the bond-breaking can not rely on phonon energy alone because the formation temperature is too low, instead an interstitial mechanism has been proposed. (9)

The interstitial mechanism is based on the correlation that metals that can diffuse interstitially in Si are the metals that can react with Si at low temperatures. The consequences of a metal atom jumping into an interstitial site in Si are that it increases the number of nearest neighbor of its surrounding host atoms and at the same time leaves a vacancy behind. The increase of the number of nearest neighbor of a Si atom weakens its bonds due to charge transfer. The weakened bonds can be regarded as being transformed from a covalent type to a metallic type. In a band picture, charge transfer from a saturated covalent bond means the formation of a hole in the valence band. While a hole is not localized at a bond as is mandated by the uncertainty principle, the bond-breaking of one particular Si atom may require the combined effect of several interstitials near the interface. Since the interface has a larger free energy than the Si lattice, it is possible that under the driving force of reaction it can take a higher concentration of interstitials.

The interstitial mechanism depends on a continuous supply of metal atoms to the silicide-silicon interface to keep the reaction going. Thus it is no surprise to find from marker studies that metal atoms are the diffusing species in the formation of all metal-rich silicides. Without free metal atoms to form interstititals, the growth will stop. The growth rate then depends on how fast can the metal atoms reach the interface. It is a diffusion limited growth and so it obeys the parabolic rule. Also because a metal-rich silicide tends to favor the diffusion of the metal atoms, the growth of a metal-rich silicide is selected. (9)

A similar interstitial mechanism has been used implicitly by Buckley and Moss (13) to explain the initial epitaxial growth of Pd_2Si on (111) surface of Si. Figure 24 is a reproduction of Fig. 5a in their paper. It shows the basal plane of Pd_2Si which has a hexagonal unit cell with a=13.055Å and c=27.490Å containing 288 atoms. The dark circles, arranged in a hexagonal net, represent Si atoms in the silicide. The net is identical to the (111) plane of Si if, the dotted, but missing, Si atoms at position A are included. For the formation of the first layer of Pd_2Si on (111) Si, we quote from their paper the following sentence, "The Pd atoms drop into the three positions around A and force the central silicon atom out of the way moving it up between them so that it nests on top of them to form the second plane of the silicide." It is obvious that the three positions around A are the interstitial sites in Si. What is also implicit in their paper is that the subsequent growth requires the same action of interstitial Pd atoms in order to remove Si from its lattice, therefore the diffusion of Pd through Pd_2Si is important. Furthermore, as we have discussed before, the diffusion of Si alone will lead to va-

cancy condensation forming voids at the Pd_2Si-Si interface and will cause a poor adhesion and impair the contact, yet Pd_2Si is known to show good adhesion and contact on Si. So, the formation of Pd_2Si can not take place by the diffusion of Si alone.

We have presented two very different pictures of growth of silicides, one for the disilicide of refractory metals and another for the metal-rich silicide of near-noble metals. It should be pointed out that some silicides seem to fall on the border lines of these two mechanisms. Notably, $CrSi_2$ can form at 450°C and Co_2Si has yet to be found to form below 350°C. It seems that until we understand how Si bonds are broken in these cases, the fine detail of the formation of these silicides can not be given.

For the monosilicides, we recall that they can be the first growth phase or their formation can be preceded by the metal-rich phase as shown in Table I. In the latter cases, the formation will be influenced by the dissociation of the preceding phase. When a monosilicide becomes the first growth phase, the mechanism of supply of Si is not clear for all the metals that fall into this class, partly because the kinetic data is not complete. We expect that the interstitial mechanism works for metals like Fe and Rh. Although the formation temperature of FeSi at 450°C is higher than the expected, it is possible that the difference in the diffusion of metal atoms through a metal-rich silicide and through a monosilicide has caused the higher formation temperature of the latter. But for Ti, Zr and Hf, while the mechanism may depend mainly on phonon energy, we suspect that there may be a small contribution to bond-breaking that comes from a direct interaction (no interstitials) between Si and these metal atoms. The inter-

action is quite strong as can be seen from the very high formation energy of their silicides as given in Table IX. The presence of some of the metal atoms at the monosilicide-silicon interface is expected. Yet the detail of the interaction is not clear at all.

4.4 Prediction of First Phase Nucleation

Walser and Bené (83) have published a rule about the first phase nucleation in silicon-transition-metal planar interfaces. The concept behind the rule is that an amorphous phase is assumed to form at the interface between the Si and metal during the deposition of the metal which resembles a fast quenching of metallic atoms onto the Si surface. Upon annealing at the silicide formation temperature, the silicide which has a concentration near that of the amorphous phase will nucleate first. The concentration of the amorphous phases is to be found near a deep eutectic point in the phase diagram, based on an earlier suggestion of Cohen and Turnbull. (84) Then the rule of Walser and Bené is to take the higher melting point silicide neighboring the deepest eutectic point (the most stable congruently melting silicide) in the binary phase diagram as the first nucleated phase.

There are several aspects of the rule and its predicted phases which require further clarification. First, the concept is based upon the formation of an amorphous phase with a rather narrow concentration range at the interface between Si and metal, yet it is known that the evaporated binary amorphous alloys can exist over a very wide concentration range. (85) Next, for the most well-established amorphous alloy of $Pd_{81}Si_{19}$, it is known that the alloy upon heat treatment transforms into the crystalline

Pd_3Si rather than the Pd_2Si as predicted. (86) The rule when applied to Pt-Si system is somewhat ambiguous; it is difficult to choose between Pt_3Si and Pt_2Si. Both are on the same side to the deepest eutectic point in the diagram. While Pt_2Si has a higher melting point, Pt_3Si is closer to the eutectic concentration. Then too, with Ni silicides, the prediction that follows the rule would be NiSi, but all measurements on Ni-Si showed Ni_2Si as the first phase to form. In private communication, Walser suggested the use of eutectoid in this case, but it remains to be shown how one can extend the concept of amorphous phase formation to a eutectoid point where no melting occurs and all the phases are solid phases. Furthermore, the prediction does not apply to the cases of Ti-Si and Mn-Si where monosilicide is the observed first growth phase rather than the predicted $TiSi_2$ and Mn_5Si_3. Finally, of course, one more difficulty is that we have been concerned with growth phase in silicide formation, yet the prediction is for the nucleation. As it has been shown by Kidson's analysis (65) that a nucleated phase could be wiped out in the growth stage due to unfavorable kinetic parameters of the growth, whether the first growth phase can be taken to be the first nucleated phase remains to be proven.

5 Conclusion

In conclusion, this report is intended to give an overview of silicide formation. Although, we obtain a very systematic pattern of silicide formation, it is clear that further work must be carried out to understand both the physical mechanism involved in silicide growth and the influence of other parameters such as stress and impurities. The present overview strongly suggests that more work is required to clarify the microstructure of silicides in terms of defects and also to clarify the nature of the

first phase that nucleates. Many of the models that we have suggested need verification. The more detailed analysis of marker motion should be pursued over a wider range of silicides. These are but a few of the areas that require fruther investigation.

References

1. M. P. Lepselter and J. M. Andrews in "Ohmic Contact to Semiconductors," edited by B. Schwartz (The Electrochemical Society, New York, 1969), p. 159.

2. T. Kawamura, D. Shinoda and H. Muta, Appl. Phys. Letters 11, 101 (1967).

3. N. G. Anantha and K. G. Ashar, IBM J. Res. & Dev. 15, 442 (1971).

4. C. J. Kircher, Solid State Electronics 14, 507 (1971).

5. H. H. Hosack, Appl. Phys. Letters 21, 256 (1972).

6. A. K. Sinha and T. E. Smith, J. Appl. Phys. 44, 3465 (1973).

7. R. J. Blattner, C. A. Evans, Jr, S. S. Lau, J. W. Mayer and B. M. Ullrich, J. Electrochem. Soc. 122, 1732 (1975).

7a. K. Takahata, K. Higuchi, T. Kubota, K. Kauchi, M. Mukogawa and H. Shiba, Extended Abs. No. 305, the 150th Electrochem. Soc. Meeting, Las Vegas, October 1976.

8. J. W. Mayer and K. N. Tu, J. Vac. Sci. Technol. 11, 86 (1974).

9. K. N. Tu, Appl. Phys. Letters 27, 221 (1975).

10. J. F. Ziegler, J. W. Mayer, C. J. Kircher and K. N. Tu, J. Appl. Phys. 44, 3851 (1973).

11. R. Feder and B. S. Berry, J. Appl. Cryst. 3, 372 (1970).

12. S. S. Lau, W. K. Chu, J. W. Mayer and K. N. Tu, Thin Solid Films 23, 205 (1974).

13. W. D. Buckley and S. C. Moss, Solid State Electron. 15, 1331 (1972).

14. S. S. Lau and D. Sigurd, Private communication.

15. J. O. Olowolafe, M-A. Nicolet and J. W. Mayer, Thin Solid Films, in press.

16. K. N. Tu, W. K. Chu and J. W. Mayer, Thin Solid Films 25, 403 (1975).

17. D. J. Fertig and G. Y. Robinson, Solid State Electron. 19, 407 (1976).

18. K. N. Tu, E. I. Alessandrini, W. K. Chu, H. Krautle and J. W. Mayer, Japan J. Appl. Phys. Suppl. 2, pt. 1, 669 (1974).

19. V. Koos and H. G. Neumann, Phys. State. Sol.(a) 29, K115 (1975).

20. K. N. Tu, J. F. Ziegler and C. J. Kircher, Appl. Phys. Letters 23, 493 (1973).

21. H. Krautle, M-A. Nicolet and J. W. Mayer, J. Appl. Phys. 45, 3304 (1974).

22. M. Hansen, "Constitution of Binary Alloys," (McGraw-Hill, New York 1959). R. P. Elliott, "Consitution of Binary Alloys, First Supplement," (McGraw-Hill, New York 1965). F. A. Shunk, "Constitution of Binary Alloys, Second Supplement," (McGraw-Hill, New York, 1969).

23. H. Kato and Y. Nakamura, Thin Solid Films 34, 135 (1976).

24. M. J. Rand and J. F. Roberts, Appl. Phys. Letters 24, 49 (1974).

25. E. I. Alessandrini, D. R. Campbell and K. N. Tu, J. Appl. Phys. 45, 4888 (1974).

26. K. N. Tu and S. Libertini, J. Appl. Phys., in press.

27. H. Krautle, W. K. Chu, M-A. Nicolet, J. W. Mayer and K. N. Tu, Proceedings of the International Conference on Applications of Ion Beams to Metals, Albuquerque, New Mexico, Plenum Press, New York 1974, p. 193.

28. W. K. Chu, private communication.

29. R. W. Bower, R. E. Scott and D. Sigurd, Solid State Electron. 16, 1461 (1973).

30. D. Sigurd, W. van der Weg, R. Bower and J. W. Mayer, Thin Solid Films 19, 319 (1974).

31. G. A. Hutchins and A. Shepala, Thin Solid Films 18, 343 (1973).

32. A. Hiraki, M-A. Nicolet and J. W. Mayer, Appl. Phys. Letters 18, 178 (1971).

33. H. Muta and D. Shinoda, J. Appl. Phys. 43, 2913 (1972).

34. J. M. Poate and T. C. Tisone, Appl. Phys. Letters 24, 391 (1974).

35. W. K. Chu, S. S. Lau, J. W. Mayer, H. Müller and K. N. Tu, Thin Solid Films 25, 393 (1975).

36. G. J. Van Gurp and C. Langereis, J. Appl. Phys. 46, 4301 (1975).

37. S. S. Lau, private communication.

38. A. K. Sinha, R. B. Marcus, T. T. Sheng and S. E. Haszka, J. Appl. Phys. 43, 3637 (1972).

39. J. M. Andrews and F. B. Koch, Solid State Electron. 14, 901 (1971).

40. S. S. Lau, J. S-Y. Feng, J. O. Olowolafe and M-A. Nicolet, Thin Solid Films 25, 415 (1975).

41. D. J. Coe, E. H. Rhoderick, P. H. Gerzon and A. W. Tinsley, "Metal-Semiconductor Contacts," Institute of Physics Conf. Ser. No. 22, London and Bristol (1974).

42. J. F. Ziegler, private communication.

43. K. E. Sundström, S. Petersson and P. A. Tove, Phys. Solid Stat. A 20, 653 (1973).

44. R. W. Bower and J. W. Mayer, Appl. Phys. Letters 20, 359 (1972).

45. C. J. Kircher and J. F. Ziegler, private communication.

46. A. G. Revesz, private communication.

47. B. I. Fomin, A. E. Gershinskii and E. I. Cherepov, Talanta, in press.

47a. B. Oertel and R. Sperling, Thin Solid Films 37, 185 (1976).

48. L. D. Locker and C. D. Capio, J. Appl. Phys. 44, 4366 (1973).

49. E. O. Kirkendall, Trans. AIME 147, 104 (1942) A. D. Smigelskas and E. O. Kirkendall, Trans. AIME 171, 130 (1947).

50. L. S. Darker, Trans. AIME 175, 184 (1948).

51. F. Brown and W. D. Mackintosh, J. Electrochem. Soc. 120, 1096 (1973).

52. W. K. Chu, H. Krautle, J. W. Mayer, H. Müller, M-A. Nicolet and K. N. Tu, Appl. Phys. Letters 25, 454 (1974).

53. G. J. van Gurp, D. Sigurd and W. F. van der Weg, Appl. Phys. Letters 29, 159 (1976).

54. S. Mader and K. N. Tu. J. Vac. Sci. Technol. 12, 501 (1975).

55. R. Pretorius, Z. L. Liau, S. S. Lau and M-A. Nicolet, Appl. Phys. Letters 29, 598 (1976).

56. R. Pretorius and S. S. Lau, private communication.

57. J. O. Olowolafe, M-A. Nicolet and J. W. Mayer, private communication.

58. C. J. Kircher, J. W. Mayer, K. N. Tu and J. F. Ziegler, Appled Phys. Letters 22, 81 (1973).

59. W. K. Chu, private communication.

60. J. A. Border and J. N. Sweet, J. Appl. Phys. 43, 3803 (1972).

61. L. C. Correa da Silva and R. Mehl, Trans AIME 191, 155 (1951).

62. D. R. Campbell, K. N. Tu and R. E. Robinson, Acta Met. 24, 609 (1976).

63. P. G. Shewmon, "Diffusion in Solids," McGraw-Hill, New York (1963).

64. J. R. Manning, "Diffusion Kinetics for Atoms in Cyrstals," Van Nostrand, Princeton (1968).

65. G. V. Kidson, J. Nucl. Mater. 3, 21 (1961).

66. A. K. Green and E. Bauer, J. Appl. Phys. 47, 1284 (1976).

67. L. S. Darken and R. W. Gurry, "Physical Chemistry of Metals," McGraw-Hill, New York 1953.

68. S. M. Hu, in "Atomic Diffusion in Semiconductors," edited by D. Shaw, Plenum Press, London & New York, 1973.

69. V. I. Tagirov and A. A. Kuliev, Soviet Phys. Solid State 4, 196 (1962).

70. R. N. Hall and J. h. Racette, J. Appl. Phys. 35, 379 (1964).

71. B. I. Boltaks and S. Y. Hsüch, Soviet Phys. Solid State 2, 2383 (1961).

72. W. R. Wilcox and T. J. LaChapelle, J. Appl. Phys. 35, 240 (1964).

73. D. Navon and V. Chernyshov, J. Appl. Phys. 28, 823 (1957).

74. R. F. Peart, Phys. Stat. Solid 15, K119 (1966).

75. B. J. Masters and J. M. Fairfield, J. Appl. Phys. 40, 2390 (1969).

76. C. B. Collins and R. O. Carlson, Phys. Rev. 108, 1409 (1957).

77. R. O. Carlson, Phys. Rev. 104, 937 (1956).

78. H. P. Bonzel, Phys. Status Solidi 20, 493 (1967).

79. R. F. Bailey and T. G. Mills, "Semiconducting Silicon," First International Symposium (Electrochem. Soc., New York, 1969) p. 481.

80. C. T. Lynch, "Handbook of Materials," CRC Press, Cleveland, (1974).

81. C. J. Smithells, "Metals Reference Book" Vol. I, 4th Edition, Plenum Press, New York (1967).

82. A. W. Searcy and A. G. Tharp, J. Phys. Chem. 64, 1539 (1960).

83. R. M. Walser and R. W. Bené, Appl. Phys. Letters 28, 624 (1976).

84. M. H. Cohen and D. Turnbull, Nature 189, 131 (1961).

85. S. Mader, Thin Solid Films 35, 195 (1976).

86. D. Gupta, K. N. Tu and K. W. Asai, Phys. Rev. Letters 35, 796 (1975).

TABLE I

Silicide Formation by Contact Reaction

Elements	Silicides		
Mg	Mg_2Si (only phase)		
Pt, Pd	Pt_2Si	PtSi (end phase)	
Ni, Co	Ni_2Si	NiSi	$NiSi_2$ (end phase)
Ti, (Zr), Hf Fe, Rh, Mn		HfSi	$HfSi_2$
V, Nb, Ta Cr, Mo, W			VSi_2

Table I Silicide Formation by Contact Reaction

TABLE II

Formation of Metal Rich Silicide, M_2Si

Silicide	Formation Temperature °C	Activation Energy of growth, eV	Growth Rate	Crystal Structure	Melting Point °C	Density* g/cm^3	References
Ni_2Si	200 ∿ 350	1.5 eV	$t^{1/2}$	Orthorhombic $PbCl_2$	1318	7.23	15,16,19
Pd_2Si	100 ∿ 700	1.3-1.5 eV	$t^{1/2}$	Hexagonal Fe_2P	1330		4,13,14,17 29,30,31
Pt_2Si	200 ∿ 500	1.1-1.6 eV	$t^{1/2}$	Tetragonal $CuAl_2$	1100		32,33,34
Mg_2Si	$\geq$ 200			Cubic CaF_2	1102		35
Co_2Si	350 ∿ 500	1.5 eV	$t^{1/2}$	Orthorhombic $PbCl_2$	1332		36,37

*Density of Si is 2.33 g/cm^3

Table II Formation of Metal-Rich Silicide

TABLE III

Formation of Monosilicide, MSi

Silicide	Formation Temperature °C	Activation Energy of Growth, eV	Growth Rate	Crystal Structure	Melting Point	Density g/cm^3	References
PtSi (end Phase)	$\geq$ 300	1.6	$t^{1/2}$	Orthorhombic MnP	1229		1,32,33, 34,38
PdSi (end Phase)	$\geq$ 700			Orthorhombic MnP	1100		31
NiSi	350-750			Cubic B20	992		18,19,39
CoSi	425-500	1.9	$t^{1/2}$	Cubic B20	1460	6.5	36,37
FeSi	450-550	1.7	$t^{1/2}$	Cubic B20	1410		40
RhSi				Cubic B20			41,42,1
HfSi	550-700	2.5	$t^{1/2}$	Orthorhombic FeB			10
TiSi	500			Orthorhombic FeB	1760	4.21	23
MnSi	400-500			Cubic B20	1275		43

Table III Formation of Monosilicide

TABLE IV

Formation of Disilicide, MSi_2

Silicide	Formation Temperature °C	Activation Energy of Growth, eV	Growth Rate	Crystal Structures	Melting Point °C	Density g/cm^3	References
$TiSi_2$	600			Orthorhombic	1540	3.9	23,44
$ZrSi_2$	700			Orthorhombic	1700		1,43
$HfSi_2$	750			Orthorhombic	1950		10
$V Si_2$	600	2.9, 1.8	t & $t^{1/2}$	Hexagonal	1750		20,21
$NbSi_2$	650			Hexagonal	1930		45
$TaSi_2$	650			Hexagonal	2200		46
$CrSi_2$	450	1.7	t	Hexagonal	1550	4.91	43,44
$MoSi_2$	525	3.2	t	Tetragonal	2050		44,47,47a
$W Si_2$	650	3	t & $t^{1/2}$	Tetragonal	2165		48,47a
$NiSi_2$	750			Cubic (CaF_2)	993		18
$CoSi_2$	550			Cubic (CaF_2)	1326		36,37
$FeSi_2$	550			Tetragonal	1212	4.54	40
$MnSi_2$	800			Tetragonal	1150		43

Table IV Formation of Disilicide

TABLE V

Metal - SiO_2 Reaction

Metallic Element, M	Metal Oxide	Metal Silicide
Au*	No	No
Al, Sn Pb	Yes	No
Pt	No	Yes
Fe, Co, Ni Cr, Mo, W V, Nb, Ta Ti, Zr, Hf	Yes	Yes

*It forms a metastable silicide. (66)

Table V Reaction Between Metal and SiO_2

TABLE VI

Comparison of Reaction Products of Ti, V and Nb on Si and SiO_2 Substrates Heat Treated in Vacuum

Elements	Substrate	Si	SiO_2 Intermediate Layer	SiO_2 Surface Layer
Ti	Backscattering	Ti:Si = 0.5	Ti:Si - 1.6	Ti:O ∿ 1
	X-ray Diffraction	$TiSi_2$	Ti_5Si_3	unidentified
	Reaction Temperature	> 500°C	> 700°C	
V	Backscattering	V:Si = 0.5	V:Si = 3	V:O ∿ 1
	X-ray Diffraction	VSi_2	V_3Si	$V_5Si_3 + V_2O_5$
	Reaction Temperature	> 500°C	> 700°C	
Nb	Backscattering	Nb:Si ∿ 1.7	Nb:Si ∿ 1.7	Nb:O ∿ 1
	X-ray Diffraction	$NbSi_2$	Nb_3Si(fcc)	unidentified
	Reaction Temperature	> 650°C	> 900°C	

Table VI Comparison of Reaction Products of Ti, V and Nb on Si and SiO_2 Substrates Heat Treated in Vacuum

TABLE VII

Marker Experiments in Silicide Formation

Element	Silicide	Dominant Diffusing Species	References
Ni	Ni_2Si	Ni	16,52
Mg	Mg_2Si	Mg	35
Co	Co_2Si	Co	53
Pd	Pd_2Si	Pd,Si	35
Pt	Pt_2Si	Pt,Si	9,34
Fe	FeSi	Si	40
Hf	HfSi	Si	58
Rh	RhSi	Si	59
Ti	$TiSi_2$	Si	35
V	$V Si_2$	Si	35

Table VII Marker Experiments in Silicide Formation

TABLE VIII

Self and Solute Diffusion Coefficient in Si

Element	$D(cm^2/sec)$	References
Cu	$4.7 \times 10^{-3} \exp(-0.43/kT)$ (300°C - 700°C)	70
Ag	$2 \times 10^{-3} \exp(-1.6/kT)$ (1100°C - 1350°C)	71
Au	$2.4 \times 10^{-4} \exp(-0.39/kT)$ (700°C - 1300°C)	72
Al	$8 \exp(-3.47/kT)$ (1085°C - 1375°C)	73
Si	$1.81 \times 10^{4} \exp(-4.86/kT)$ (900°C - 1300°C)	74,72
As	$60 \times \exp(-4.2/kT)$ (850°C - 1150°C)	75
Cr	$< 10^{-8}$ (1200°C)	76
Mn	$> 2 \times 10^{-7}$ (1200°C)	77
Fe	$> 5 \times 10^{-6}$ (100°C - 1115°C)	76
Ni	1.57×10^{-7} (800°C)	78
Pt	Similar to Au in Si	79

Table VIII Self and Metallic Solute Diffusion Coefficients in Si

TABLE IX

Free Energy of Formation of Silicides

ΔH, Kcal/g - atom

(Data from H.B. of Materials, Smithells', and Searcy and Finnie)

Mg_2Si - 6.2	Ti_5Si_3 - 17.3	V_3Si - 6.5
	TiSi - 15.5	V_5Si_3 - 11.8
FeSi - 8.8	$TiSi_2$ - 10.7	V Si_2 - 24.3
$FeSi_2$ - 6.2		
	Zr_2Si - 16.7	Nb_5Si_3 -10.9
Co_2Si - 9.2	Zr_5Si_3 - 18.3	$NbSi_2$ -10.7
CoSi - 12	ZrSi - 18.5,17.7	
$CoSi_2$ - 8.2	$ZrSi_2$ - 12.9,11.9	Ta_5Si_3 -9.5
		$TaSi_2$ -8.7,9.3
Ni_2Si - 11.2,10.5	HfSi	
NiSi - 10.3	$HfSi_2$	Cr_3Si -7.5
		Cr_5Si_3 -8
Pd_2Si - 6.9		CrSi -7.5
PdSi - 6.9		$CrSi_2$ -7.7
		Mo_3Si -5.6
Pt_2Si - 6.9		Mo_5Si_3 -8.5
PtSi - 7.9		$MoSi_2$ -8.7,10.5
RhSi - 8.1		W_5Si_3 -5
		WSi_2 -7.3

Table IX Formation Energy of Silicides

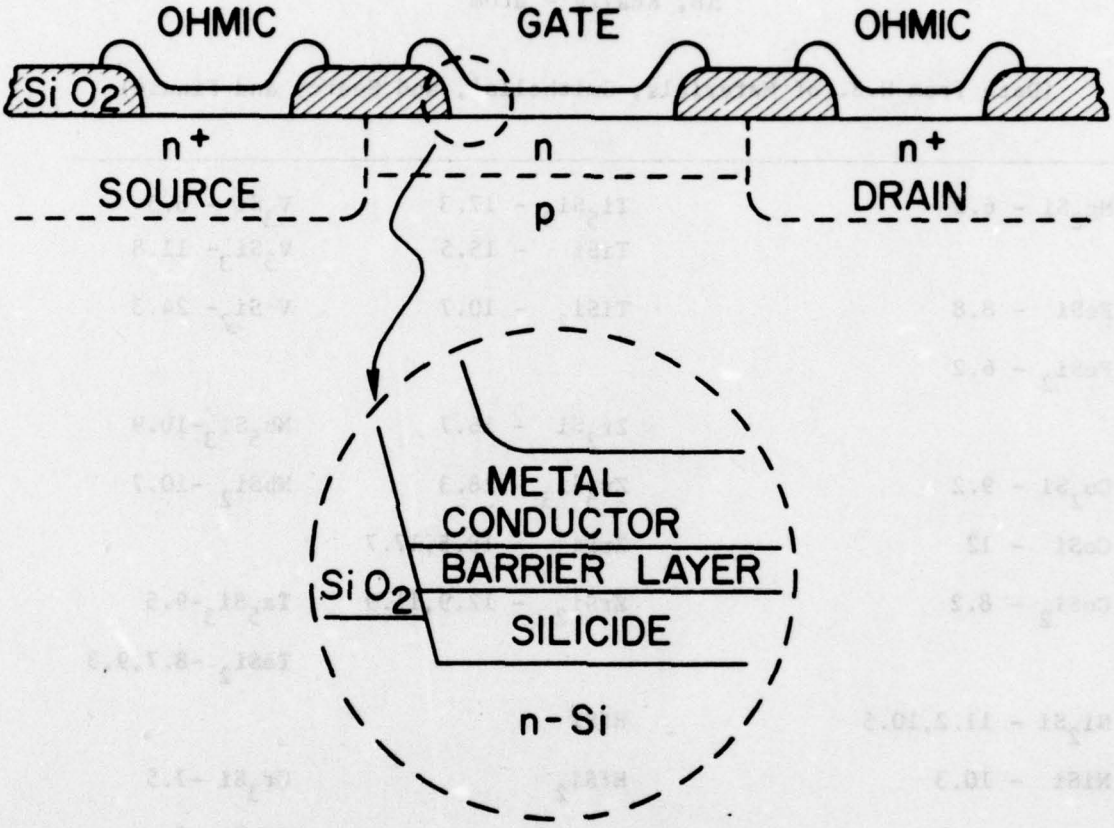

Fig. 1. A schematic FET structure.

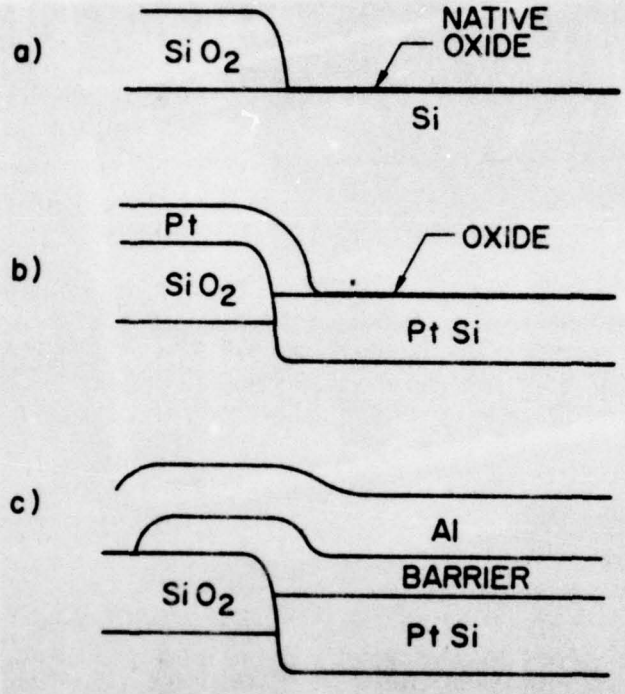

Fig. 2. Schematic metallization steps in forming a silicide contact on Si.

a) Oxide window before Pt deposition.
b) Sintering to complete PtSi formation.
c) The contact structure after barrier and Al deposition.

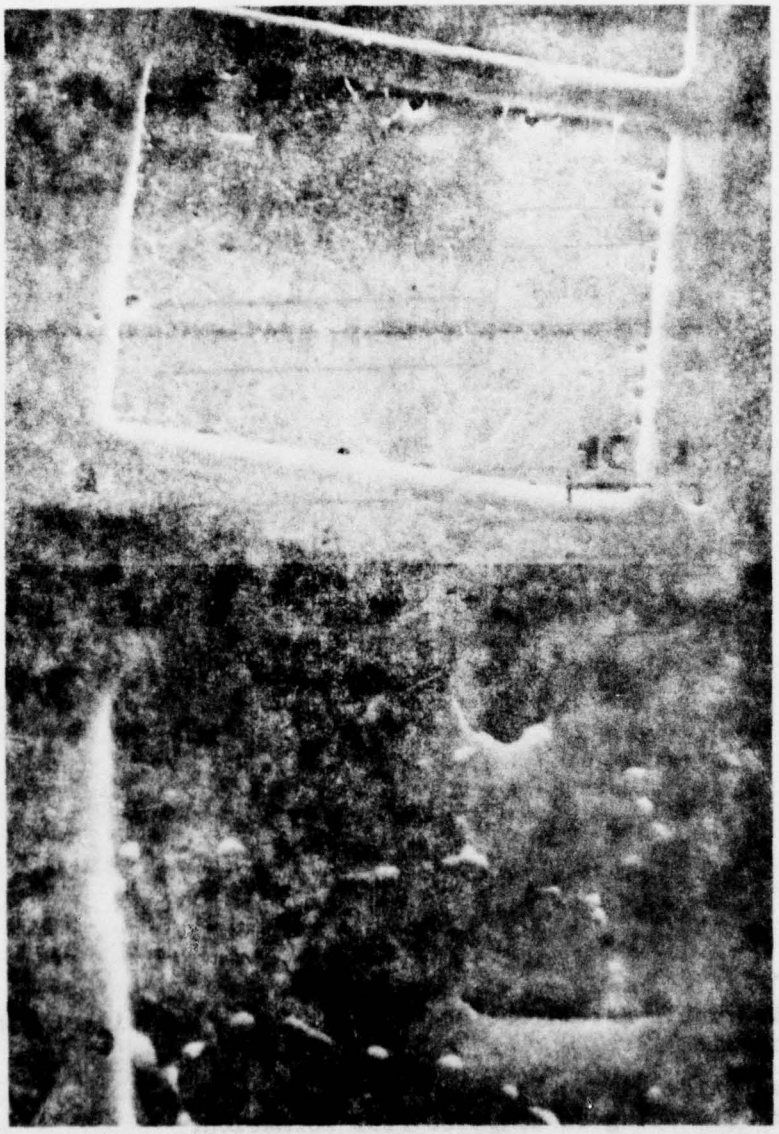

x1600

x8000

Fig. 3. SEM micrographs of spike formation around the periphery of a contact area.

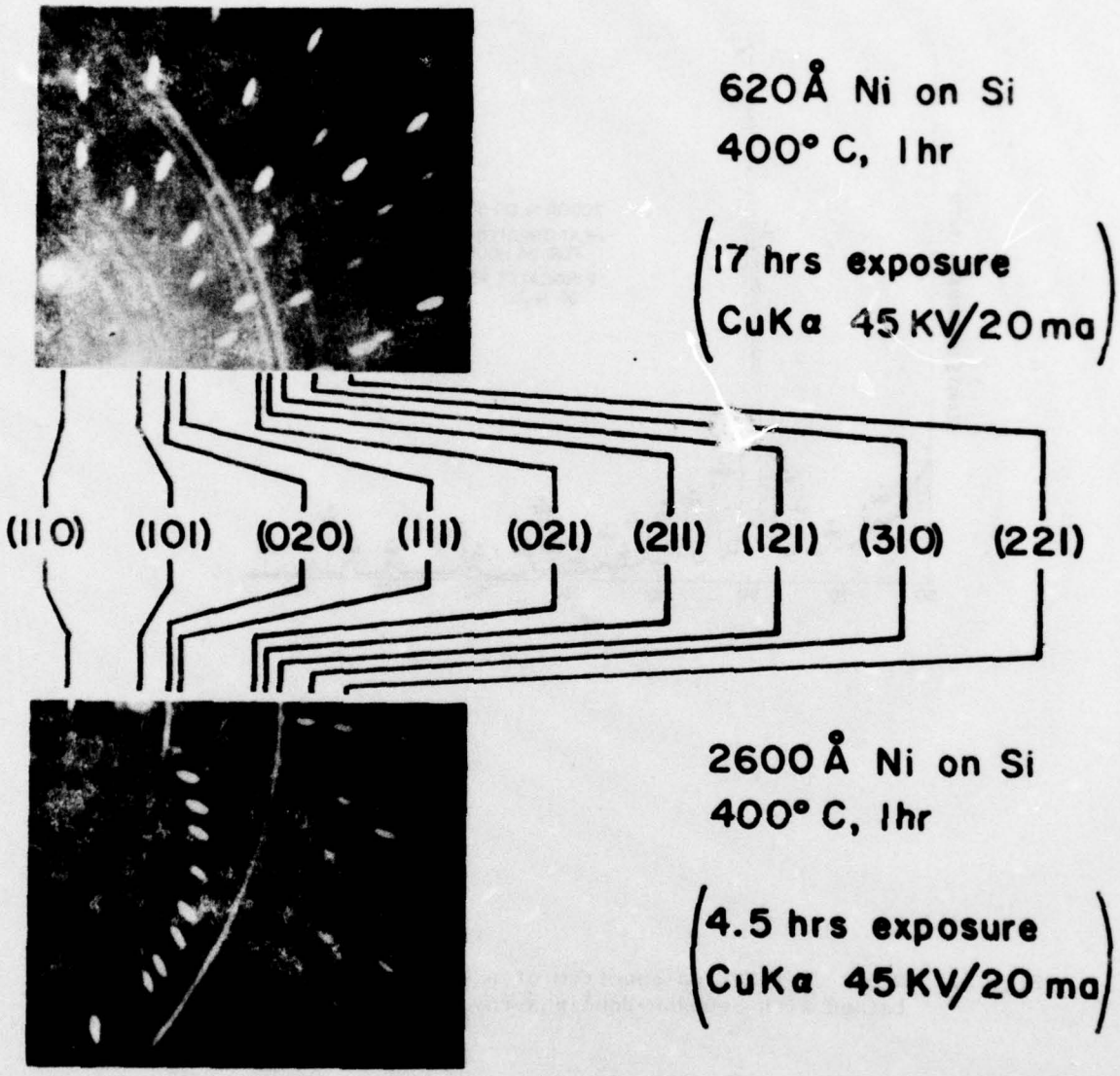

Fig. 4. X-ray diffraction pattern of a NiSi film obtained with a Reed camera.

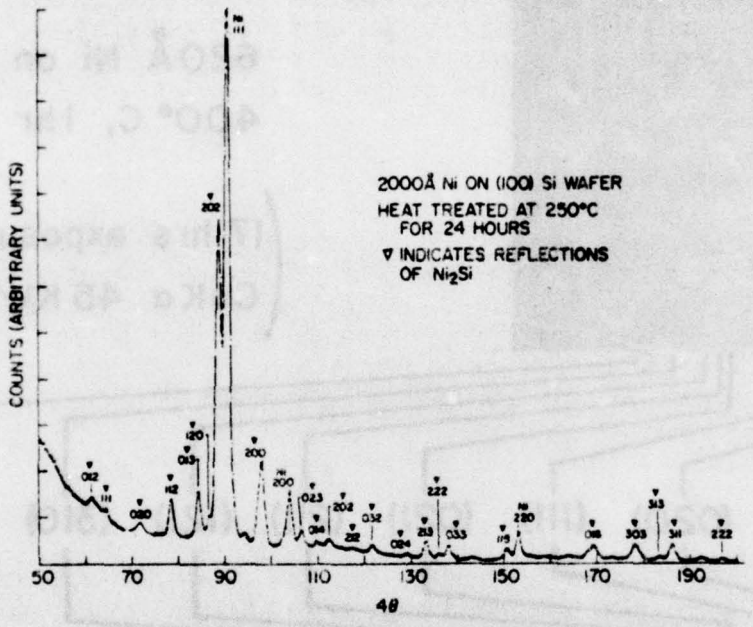

Fig. 5. X-ray diffraction spectrum of a heat treated Ni film on Si obtained with Seemann-Bohlin x-ray diffractometer.

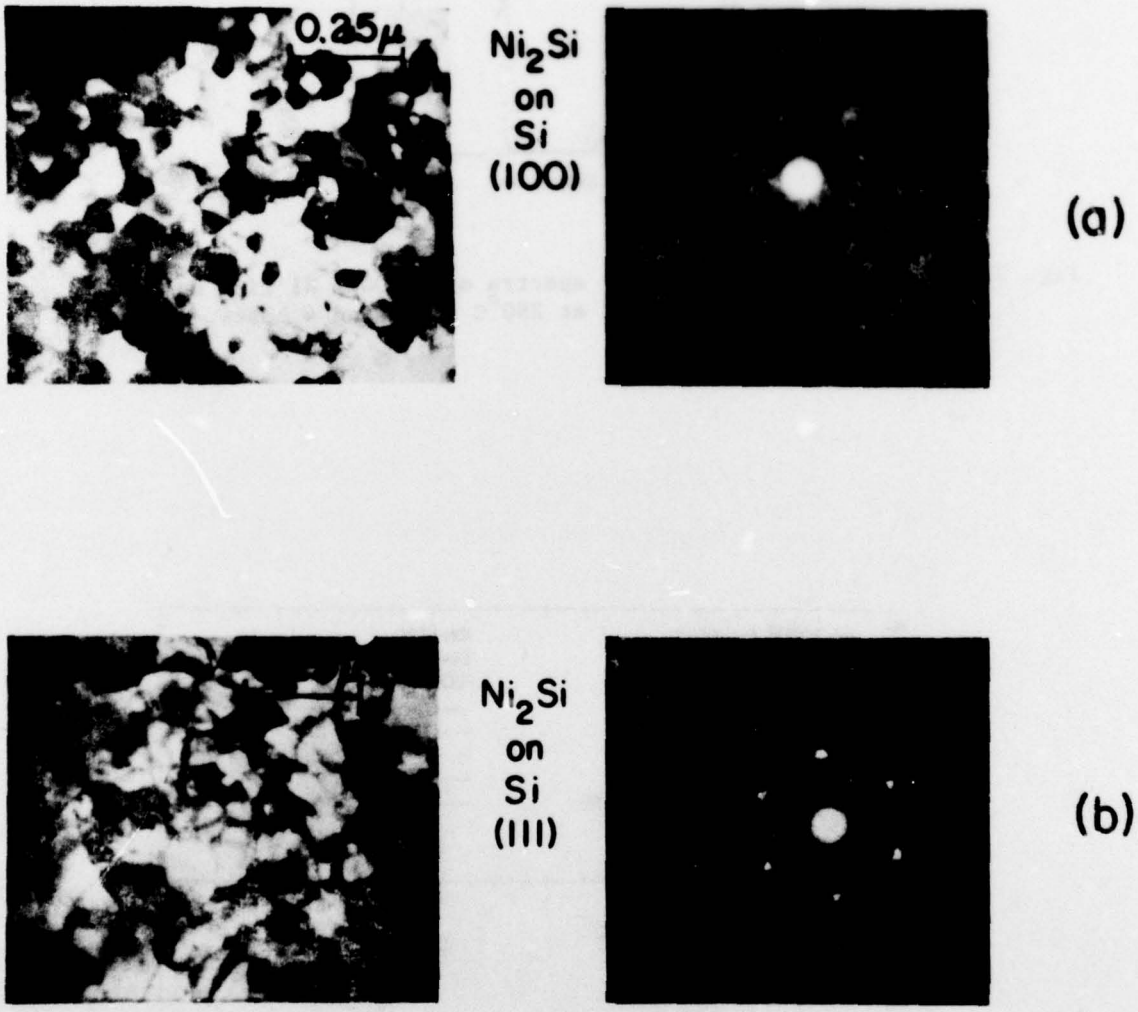

Fig. 6. Transmission electron micrographs and diffraction patterns of Ni_2Si formed by 1600Å of Ni (a) on (100) Si and annealed at 300°C for 5 hrs. and (b) on (111) Si and annealed at 325°C for 580 min. The average grains size of Ni_2Si is about 600Å in (a) and 1300 to 1400Å in (b). The diffraction patterns in the latter case indicates that the Ni_2Si is textured.

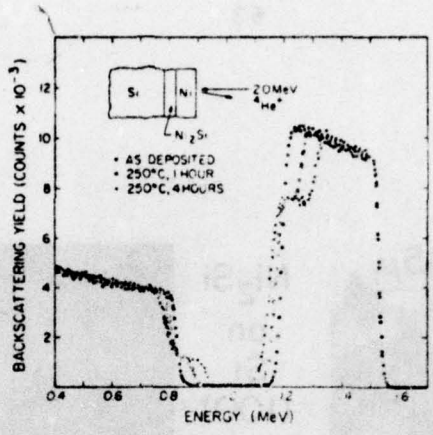

Fig. 7. Rutherford backscattering spectra of a 2000Å Ni film on Si before and after annealed at 250°C for 1 and 4 hours.

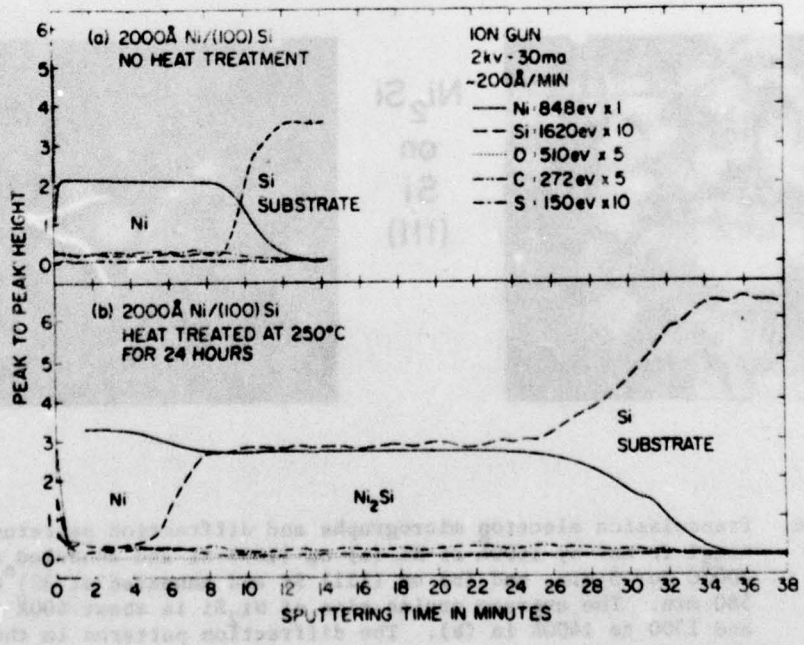

Fig. 8. Auger depth profiles of a sample of Ni film on Si before and after the reaction at 250°C for 1 hour to form the silicide Ni_2Si.

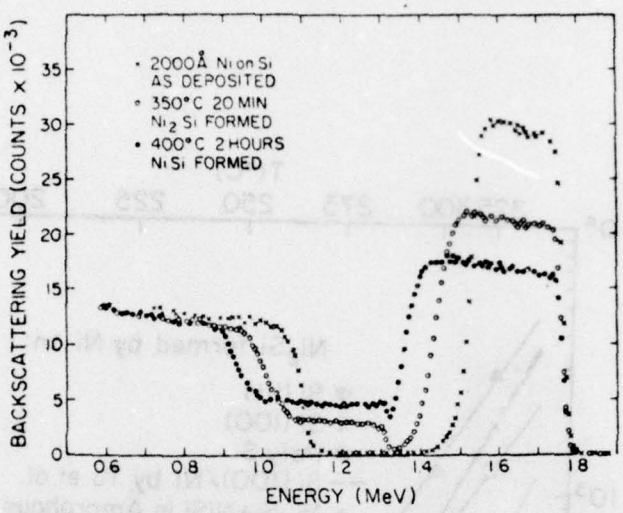

Fig. 9. Backscattering spectra of a sample of Ni on Si showing the sequential formation of Ni_2Si and NiSi.

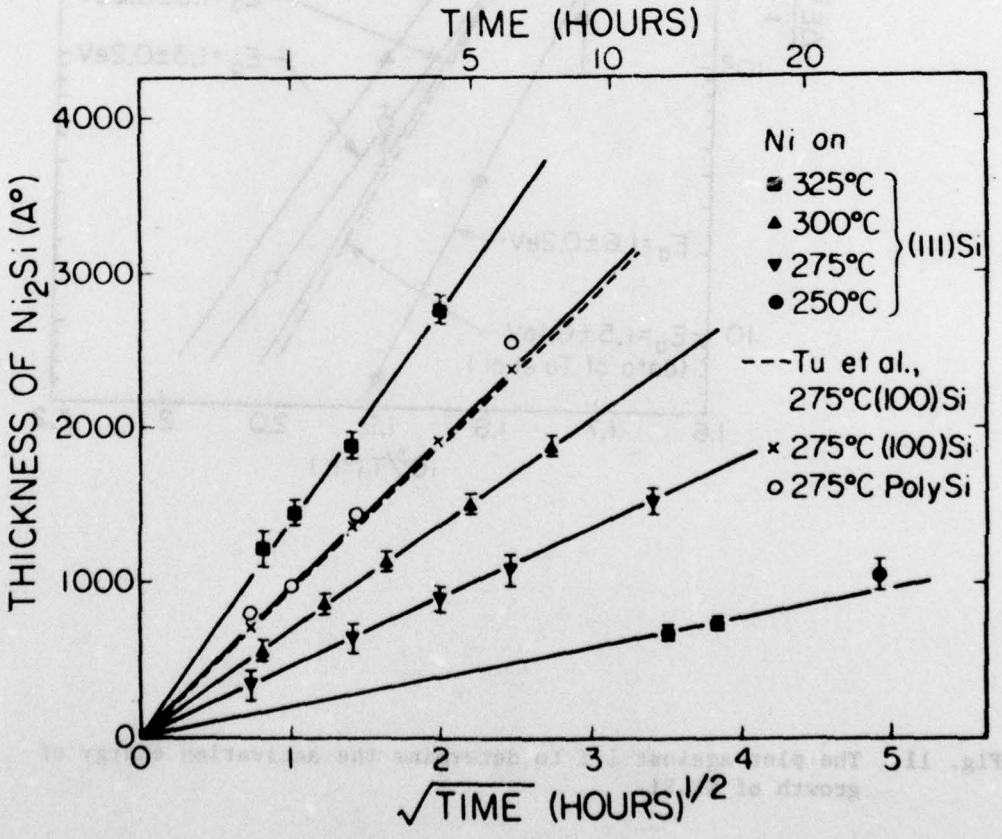

Fig. 10. Data of parabolic growth of Ni_2Si.

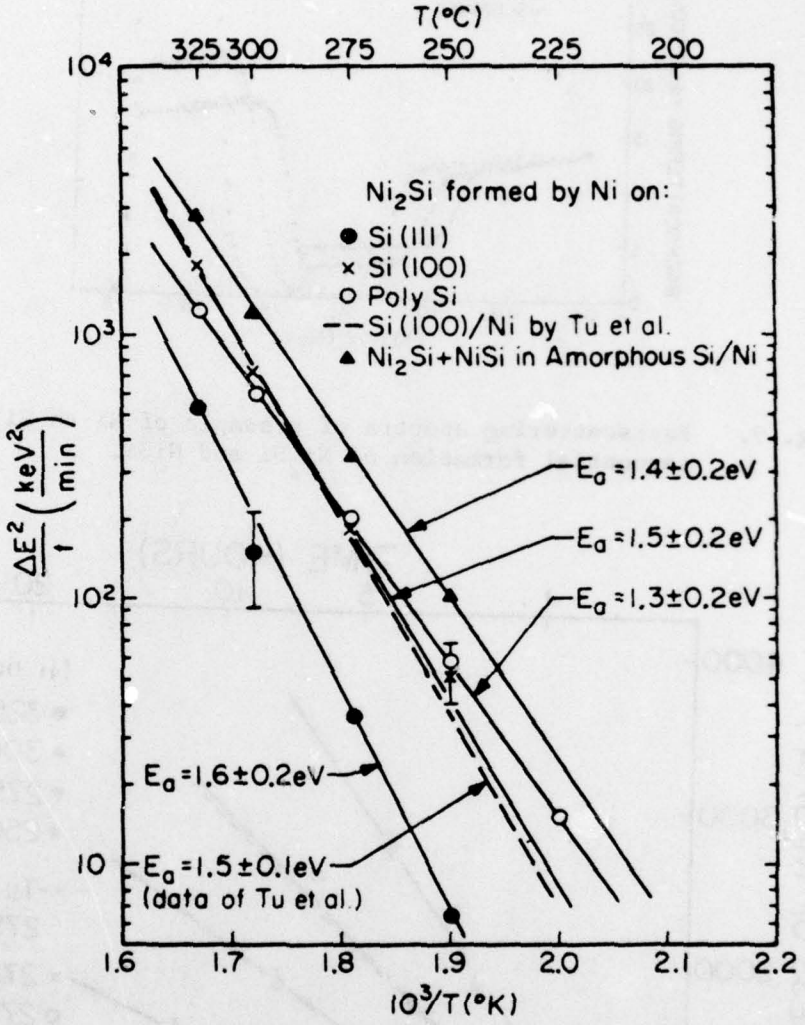

Fig. 11. The plot against 1/T to determine the activation energy of growth of Ni_2Si.

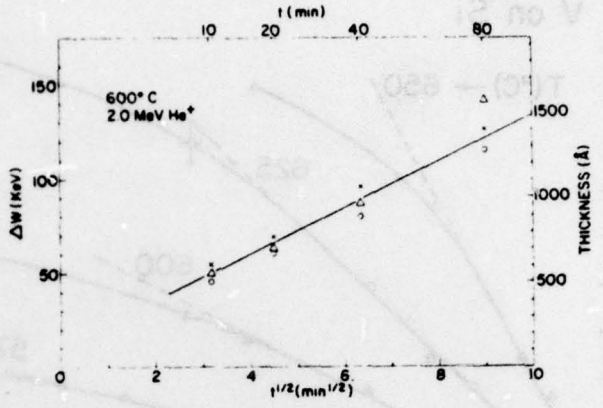

Fig. 12. The width ΔW of the plateaus in the Hf peak as a function of $(\text{time})^{1/2}$ for three 1500Å Hf films deposited on <100> (X) and <111> (0) Si at $\sim$ 200°C and on <100> Si at $\sim$ 400°C (Δ).

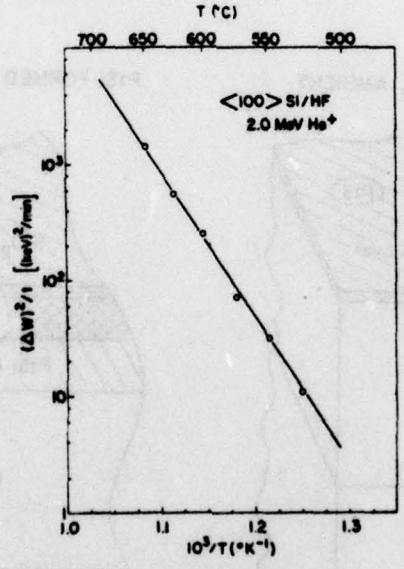

Fig. 13. The plot of $(\Delta W)^2/t$ against 1/T to determine the activation energy of growth of HfSi.

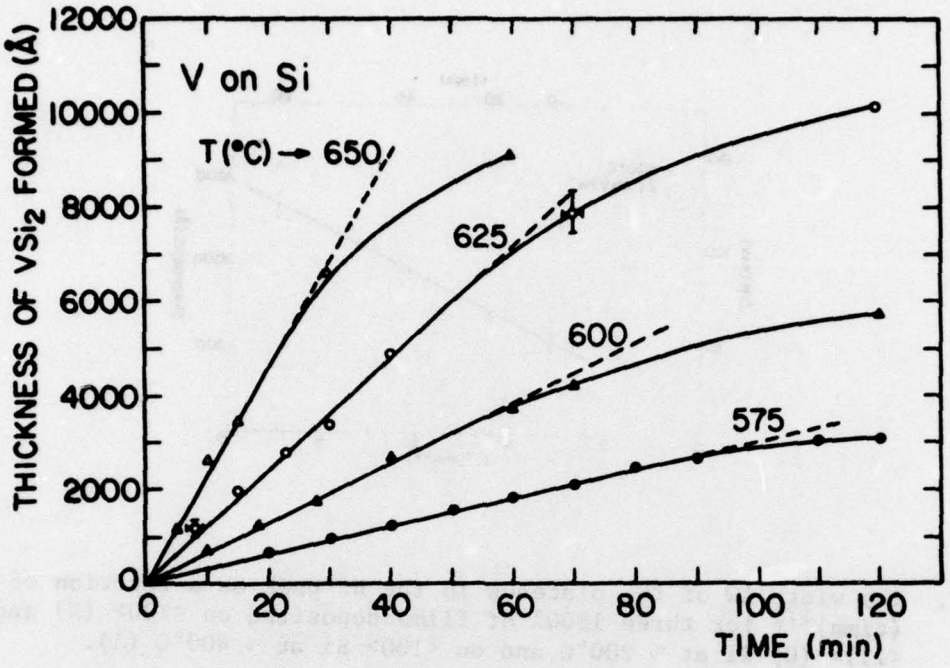

Fig. 14. Data of linear growth of VSi_2.

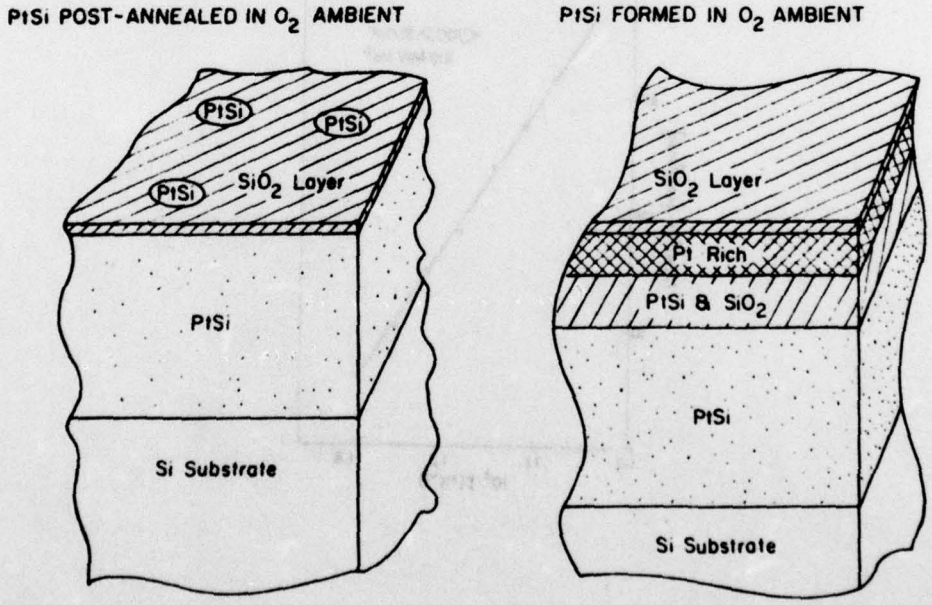

Fig. 15. Schematic diagrams of oxide layer formation during the growth of PtSi in an oxygen ambient or post-annealed in oxygen.

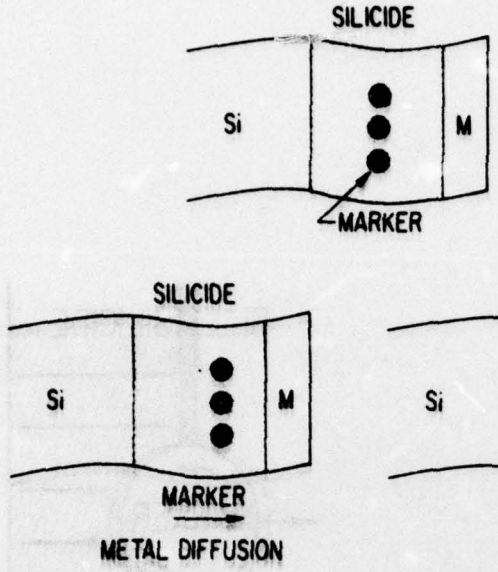

Fig. 16. Schematic diagram of marker motion in silicide formation.

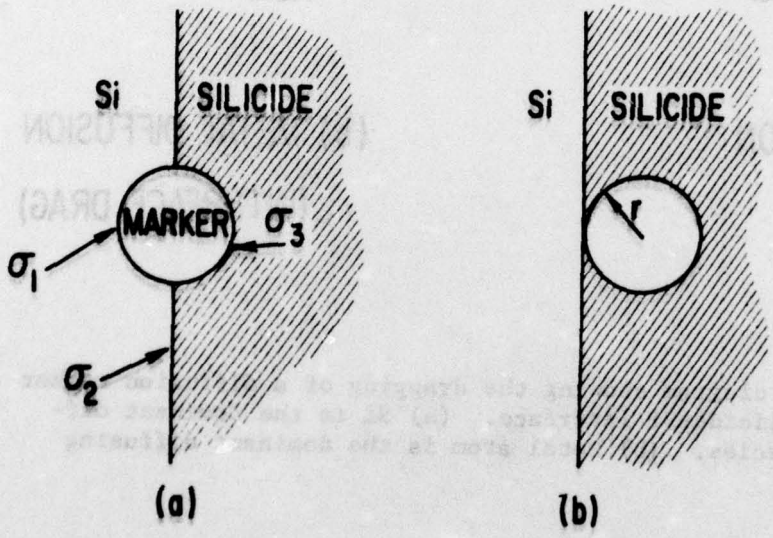

Fig. 17. Schematic diagram of a spherical marker (a) at the silicide-Si interface and (b) to be buried in the silicide.

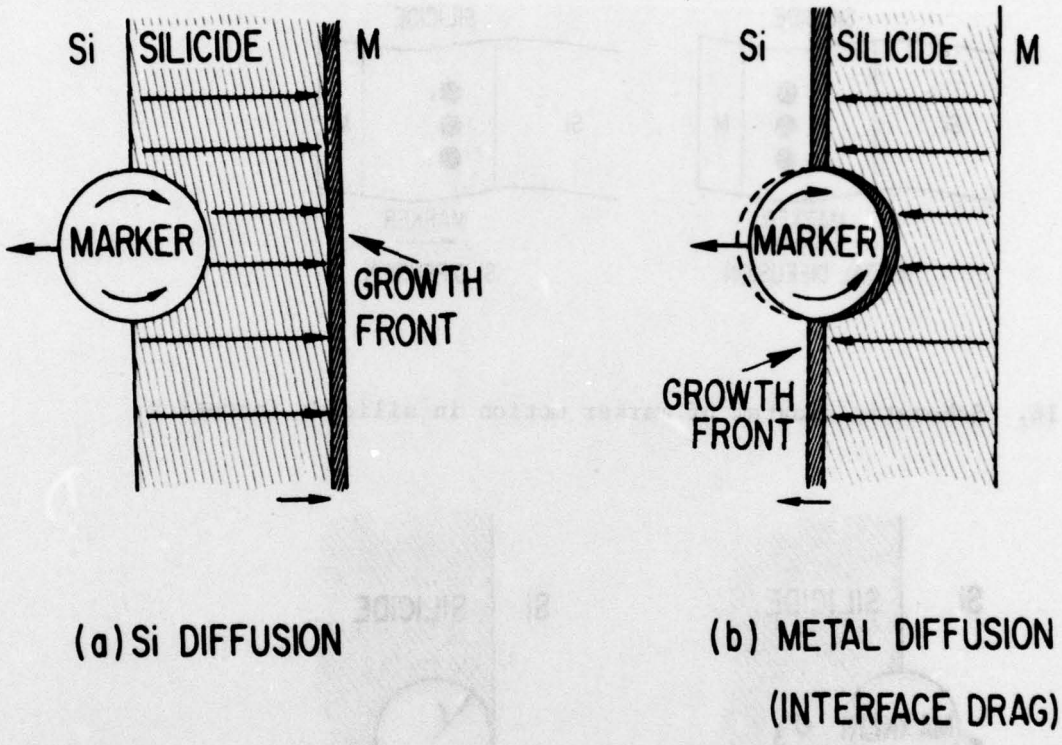

Fig. 18. Schematic diagram showing the dragging of a diffusion marker by the silicide-Si interface. (a) Si is the dominant diffusing species. (b) Metal atom is the dominant diffusing species.

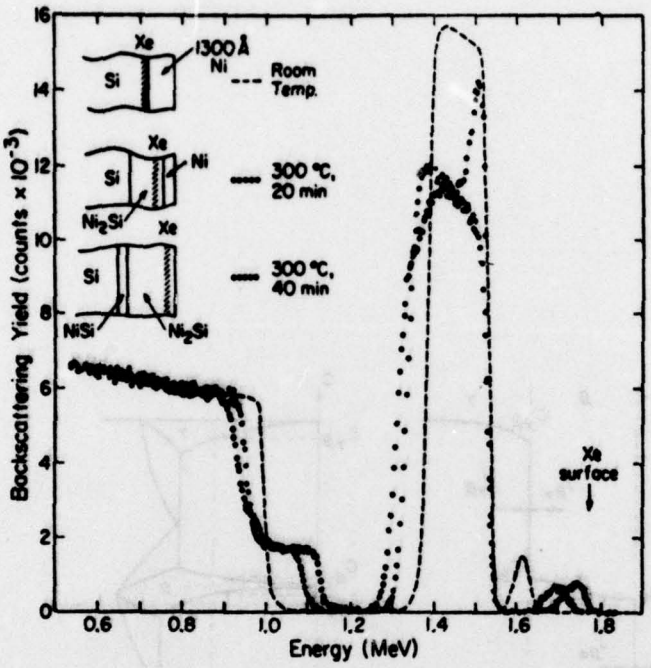

Fig. 19. (a) Marker motion during the formation of Ni_2Si.

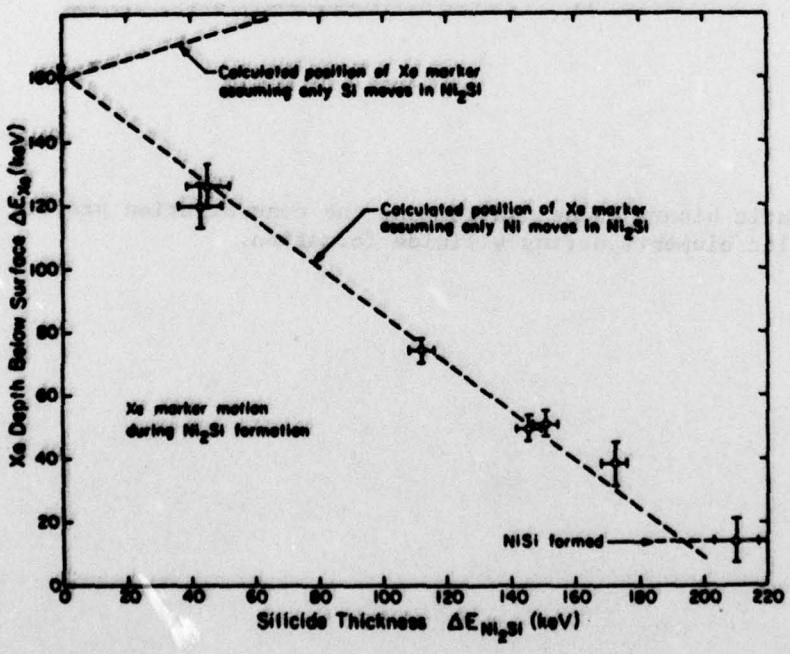

(b) The amount of Xe marker displacement against the silicide thickness.

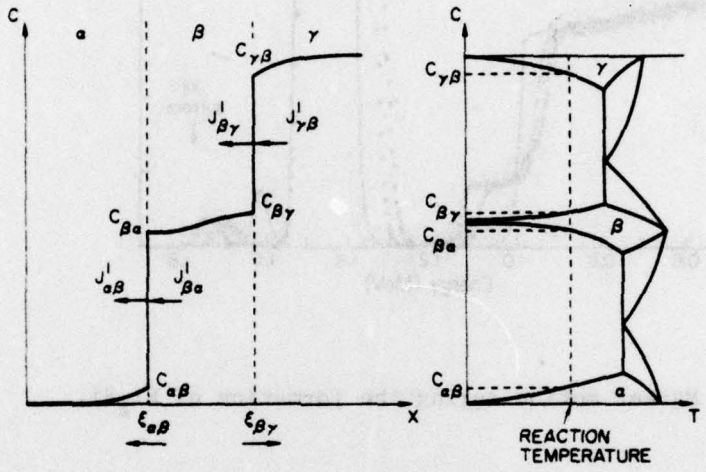

Fig. 20. Schematic binary phase diagram and the concentration profile of metallic elements during silicide formation.

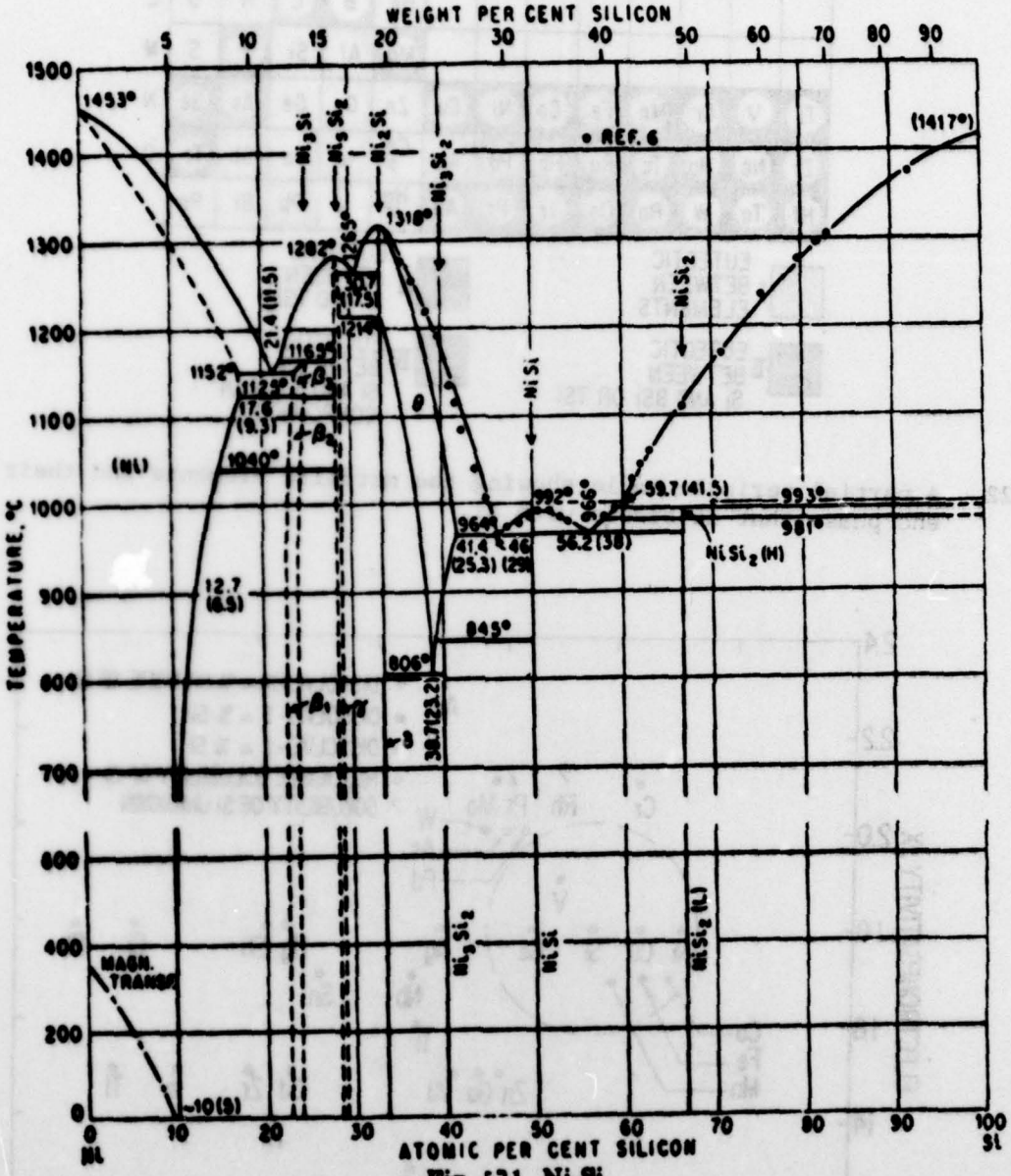

Fig. 571. Ni-Si

Fig. 21. Binary phase diagram of Ni-Si.

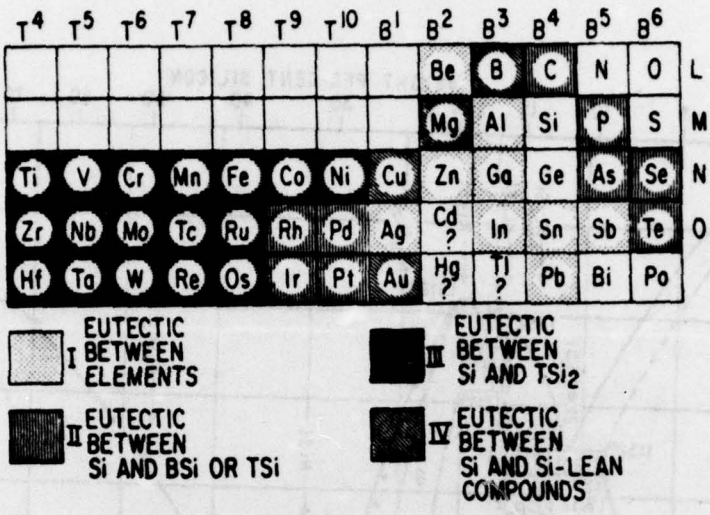

Fig. 22. A partial periodic table showing the metallic elements and their end phase that is stable with Si.

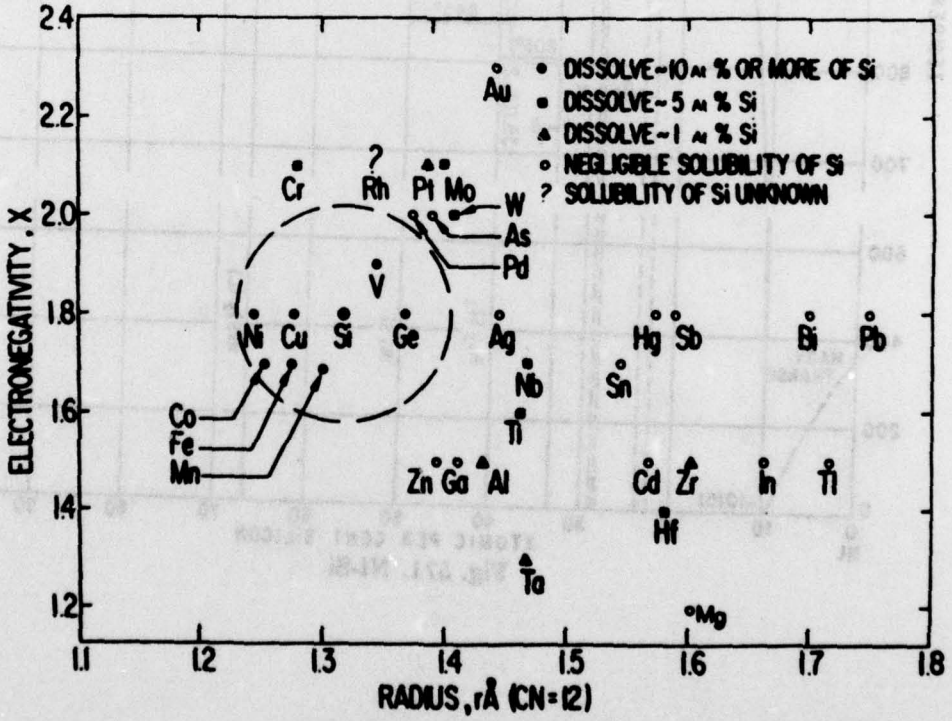

Fig. 23. Darken and Gurry plot of electronegativity vs. atomic radius to show the solubility of Si in various metals.

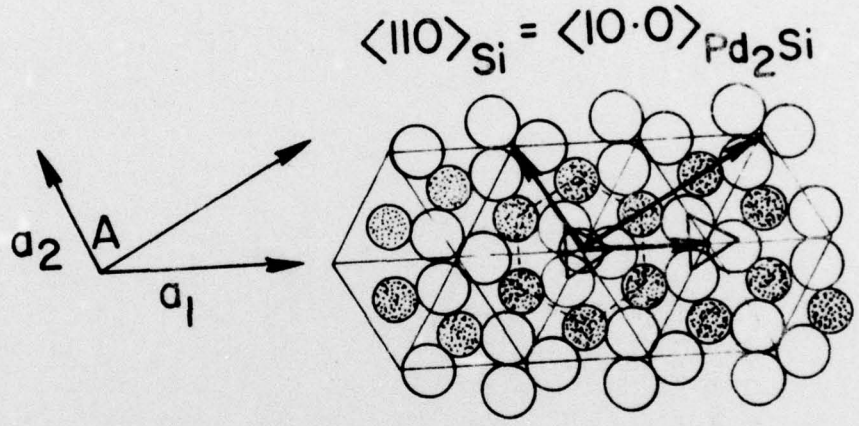

Fig. 24. Atomic arrangement in the basal plane of Pd_2Si.